into normal 24-well plates (BD Biosciences) and grown for 24 h. Three μl of HyperFect Reagent (Qiagen), 100 μl of F12-K FBS free medium and siRNA (25 nM) were mixed, incubated at room temperature for 5 min and added to cells. After 96 h, cells were used for analysis and experimentation. A549 cells transfected with siRNA were washed with sterile PBS and total RNA was extracted with Isogen reagent (Bio-Rad Laboratories, Hercules, CA) according to the manufacturer's protocol. After deoxyribonuclease treatment, total RNA (1 μg) of A549 cells was reverse-transcribed using Improm-II™ reverse transcriptase (Promega, Madison, WI) and oligo (dT). A mixture of 1 μl of oligo (dT) (0.5 μg/μl) and total RNA (1 μg) was incubated at 70°C for 5 min, then rapidly chilled at 4°C for 5 min. For conversion of total RNA to cDNA, the reaction mixture (20 μl) was prepared containing the mixture of oligo (dT) and total RNA, 4 μl of 5×RT buffer, 2.4 μl of 25 mg $MgCl_2$, 4 μl of 2.5 mM dNTP mix, 0.5 μl of Rnasin (1 U/μl), 1 μl of Improm-II reverse transcriptase and 3.1 μl of diethylpyrocarbonate-treated water. The reaction was carried out at 25°C for 5 min, 42°C for 60 min and 70°C for 15 min. RT reaction mixtures, including cDNA products, were stored at −20°C until used. A single cDNA produced from total RNA was amplified by quantitative PCR with FullVelocity SYBER Green QPCR Master Mix (Strategene, Tokyo, Japan KK) and specific primers for CTL1 (QT00075838, Qiagen) and GAPDH (forward: '5-GAAGGTGAAGGTCGGAGT-3' and reverse: '5-GAAGATGGTGATGGGATTTC-3'). A two-step temperature program was applied for the amplification of hCTL1 and GAPDH: initial denaturation (95°C) for 10 min, then 95°C for 15 s, 60°C for 60 s for 50 cycles.

Kinetic Analyses

Uptake was expressed as the cell-to-medium ratio (μl/mg protein) obtained by dividing the uptake amount by the concentration of substrate in the incubation buffer. Specific uptake was obtained by subtracting the uptake at 4°C from the uptake at 37°C. Kinetic parameters were obtained using the following equation (Eq. 1):

$$v = \frac{V_{max} \times S}{K_m + S} \quad (1)$$

where v is the uptake velocity of the substrate (pmol/30 s/mg protein), S is the substrate concentration in the medium (μM), K_m is the Michaelis constant (μM) and V_{max} is the maximum uptake rate (pmol/30 s/mg protein). Fitting was performed by the nonlinear least-squares method using a computer program (WinNonlin program, Pharsight, USA). The half-inhibitory concentration (IC_{50}) of inhibitors was obtained by examining their inhibitory effects on the uptake of choline based on Eq. 2.

$$\frac{C}{M_{+I}} = \frac{C}{M} \Big/ \left(1 + \left(\frac{I}{IC_{50}}\right)^H\right) \quad (2)$$

where C/M and C/M_{+I} represent the uptake clearance in the absence and presence of inhibitor, respectively. H is the slope factor and I is the concentration of inhibitor. IC_{50} values were estimated by the nonlinear least-squares method using a computer program (WinNonlin program, Pharsight, USA).

Statistical Analysis

Student's t-test was used to assess the significance of differences between two sets of data. Differences were considered to be statistically significant when p was <0.05.

RESULTS

Inhibitory effect of gefitinib on PC biosynthesis in A549 and primary-cultured rat ATII cells. To examine whether gefitinib reduces PC biosynthesis in A549 and primary-cultured rat ATII cells, the effect of gefitinib on the CDP-choline pathway was examined. In both A549 and rat ATII cells, [^{3}H]choline was incorporated into PC in a time-dependent manner over 3 h (Fig. 2a and d). Twenty and 50 μM gefitinib reduced the apparent uptake of [^{3}H]choline to 53.6±2.36 and 70.7±4.50% in A549 and rat ATII cells, respectively, compared to the values in the absence of gefitinib (Fig. 2b and e). In addition, the radioactivity in the chloroform phase from A549 and rat ATII cells, containing only PC, was decreased by 20 and 50 μM gefitinib to 57.7±7.33 and 64.1±2.56%, respectively (Fig. 2b and e). Furthermore, preincubation of 20 and 50 μM gefitinib with those cells for 60 min exhibited stronger reductions of apparent uptake and incorporation into PC of [^{3}H]choline (uptake by the cells: 47.9±3.11 and 11.1±0.794%; PC biosynthesis: 30.5±7.90 and 1.44±0.131% for A549 and rat ATII cells, respectively) (Fig. 2c and f). These results demonstrated that gefitinib inhibits the apparent uptake of choline and the subsequent biosynthesis of PC, and its effect is significantly increased when the cells are pretreated with the drug.

Characteristics of [^{3}H]choline transport in A549 and primary-cultured rat ATII cells. [^{3}H]Choline was taken up linearly by A549 cells up to 1 min, and the uptake showed temperature dependence (37°C: 40.2±4.12 μl/30 s/mg, 20°C: 21.5±1.57 μl/30 s/mg, 4°C: 8.12±1.00 μl/30 s/mg). The initial uptake of choline by A549 cells was studied over the concentration range from 0.1 to 50 μM. The Eadie-Hofstee plot showed a single saturable component and the apparent K_m and V_{max} values were 15.0±1.15 μM and 314±18.2 pmol/30 s/mg, respectively. Similarly, [^{3}H]choline was taken up linearly by rat ATII cells up to 5 min and the initial uptake at 2 min was temperature-dependent (37°C: 54.1±3.25 μl/2 min/mg, 4°C: 16.7±3.42 μl/2 min/mg). The temperature-dependent [^{3}H]choline uptake was almost completely inhibited by unlabeled 100 μM choline, showing that the uptake is saturable ([^{3}H]choline alone (1 μM): 37.4±3.25 μl/2 min/mg, with unlabeled choline 10 μM: 18.9±3.37 μl/2 min/mg, 100 μM: 1.66±2.73 μl/2 min/mg). Decrease of Na^+ and K^+ in the incubation media reduced the uptake of [^{3}H]choline by A549 cells (Fig. 3a, b and d). The uptake of [^{3}H]choline by A549 cells was found to be markedly increased by changing the extracellular pH from 5.5 to 8.5 (Fig. 3c). [^{3}H]Choline uptake by rat ATII cells was weakly reduced by replacement from Na^+ to NMG^+ in the incubation media as well as A549 cells (Fig. 3e). The uptake of [^{3}H]choline was not affected by corticosterone, histamine or MPP^+, which are substrates and

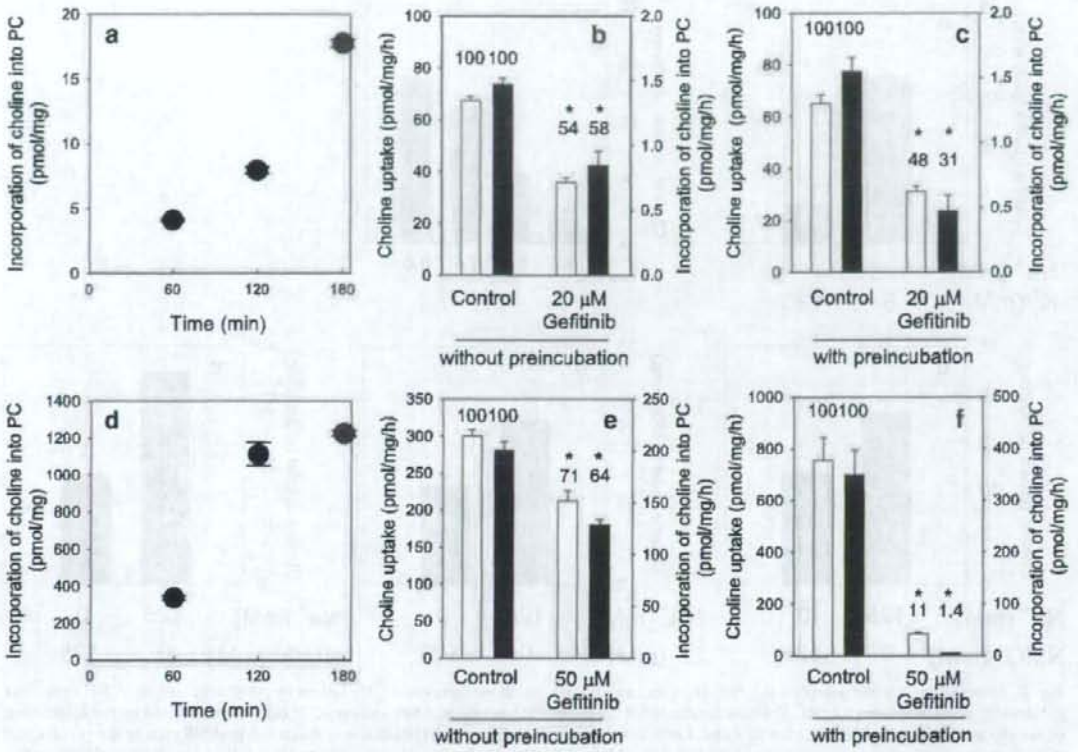

Fig. 2. Time profile of incorporation of [^{3}H]choline into PC in A549 cells (**a**) and rat primary-cultured ATII cells (**d**), and inhibitory effect of gefitinib on the apparent uptake and incorporation of [^{3}H]choline into PC by A549 (**b** and **c**) and rat primary-cultured ATII cells (**e** and **f**) with (**c** and **f**) or without preincubation (**b** and **e**). The concentration of [^{3}H]choline was 0.1 μM. (**b**, **c**, **e**, **f**) *Open* and *filled bars* indicate the apparent uptake by the cells and PC in the chloroform phase (which corresponds to incorporation into PC), respectively. Values above bars are percentages of apparent uptake and PC in the chloroform phase in the absence of gefitinib. The inhibitory effect of gefitinib on the incorporation of [^{3}H]choline into PC by A549 and rat ATII cells was measured at 37°C for 1 h. The preincubation of A549 and rat ATII cells with gefitinib for 1 h was carried out prior to the PC biosynthesis. * $p<0.05$ compared with control. Each point and bar represents the mean ± S.E. from at least 3 wells.

inhibitors of human OCT1, 2, and 3, whereas HC-3, a choline analogue, inhibited the [^{3}H]choline uptake by A549 and rat ATII cells in a concentration-dependent manner with IC_{50} values of 9.48±1.06 μM (Fig. 4a) and 79.9±17.9 μM (Fig. 4b), respectively.

Identification of transporters expressed in A549 and primary-cultured rat ATII cells. To investigate what transporter molecules are expressed in A549 and primary-cultured rat ATII cells and to compare the expression profile in A549 and rat ATII cells with those in human bronchial epithelial Calu-3 cells, lung, trachea, liver and kidney and in rat lung, liver and kidney (Fig. 5), the expression of transporter mRNAs was examined by RT-PCR. The experimental conditions used for RT-PCR were validated by demonstrating the formation of RT-PCR products of the expected sizes for OCTs and CTLs with total RNAs of liver and kidney from rat and human as positive controls. Under these conditions, RT-PCR did not show the expression of human or rat OCT2 in A549, Calu-3, lung, trachea, rat ATII cells and or rat lung. In rat ATII cells, very weak mRNA expression of OCT1 was observed. The expression of human and rat OCT3 was observed in all tissues examined, except for human liver. The expression of human CTL1 mRNA was confirmed in all tissues, but the expression levels in trachea, liver and kidney were very low. The expression of rat CTL1 mRNA was observed in all tissues examined. Although mRNA of CTL2 was found in Calu-3, lung, trachea, liver and kidney, it was not detected in A549 cells.

Effect of hCTL1 siRNA on hCTL1 mRNA expression and [^{3}H]choline uptake in A549 cells. We investigated whether hCTL1 knockdown induced any change in hCTL1 mRNA expression and [^{3}H]choline transport in A549 cells (Fig. 6a and b). Firstly, we checked whether the negative control siRNA from Qiagen was suitable as a negative control for hCTL1. The negative control siRNA did not decrease hCTL1 mRNA expression compared with that in the cells transfected only with the transfection reagent, at 48, 72 and 96 h after transfection (data not shown). Thus, we used this siRNA as the negative control in the present study. The hCTL1 mRNA expression level and [^{3}H]choline uptake by A549 cells were determined 96 h after siRNA transfection in A549 cells. The expression of hCTL1 mRNA in A549 cells

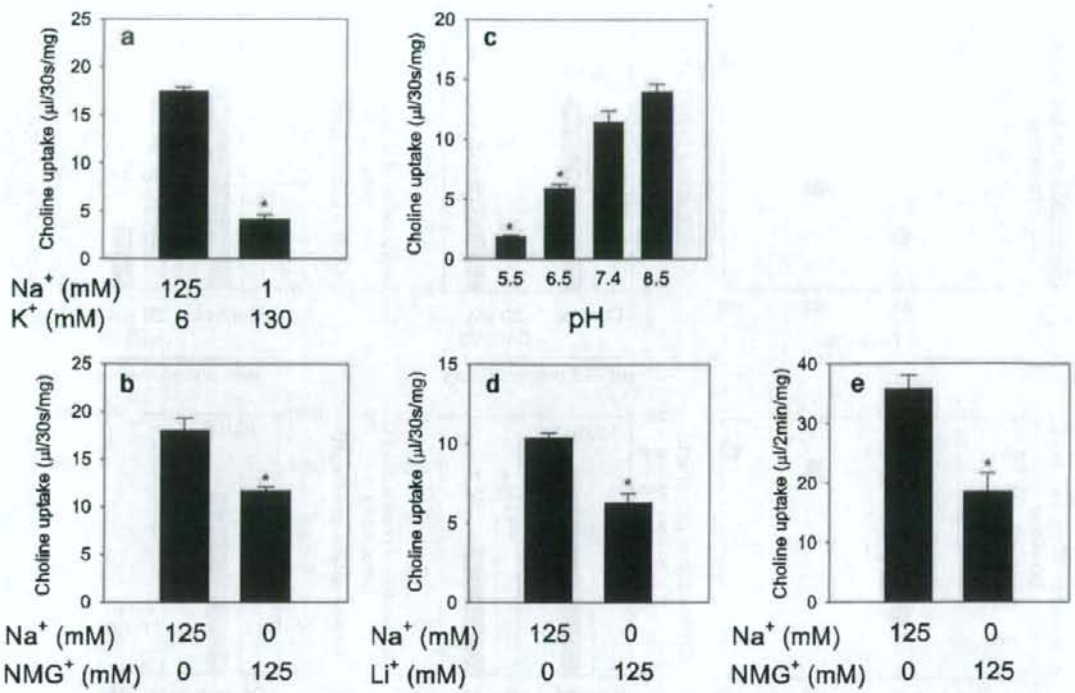

Fig. 3. Effect of membrane potential (**a**), Na^+ (**b**, **d** and **e**), and pH (**c**) on the uptake of [^{3}H]choline by A549 cells and rat AT II cells. The substrate concentration was 0.1 μM. Transporter-mediated uptake of [^{3}H]choline in A549 and rat ATII cells was calculated by the subtraction of uptake at 4°C from that at 37°C for 30 s and 2 min, respectively. **a** Uptake of [^{3}H]choline was measured in A549 cells in the presence of increasing and decreasing concentrations of KCl (6–130 mM) and NaCl (125–1 mM), respectively, at pH 7.4. **b** and **d** Uptake of [^{3}H]choline was measured in A549 cells (**b** and **d**) and rat ATII cells (**e**) in Na^+-free buffer. In Na^+-free buffer, the NaCl in the incubation buffer was replaced with N-methylglucamine (NMG) and lithium chloride at pH 7.4. **c** Uptake of [^{3}H]choline was measured in A549 cells in the various pH of the incubation buffer varied by adjusting the concentrations of Mes, Hepes and Tris. * $p<0.05$ compared with the uptake in normal incubation buffer at pH 7.4. Each bar represents the mean + S.E. from at least 3 wells.

and the [^{3}H]choline uptake by A549 cells were decreased by the transfection of three different siRNAs to 38.6–66.4% and 34–50%, respectively, compared with the values obtained with the negative control siRNA. To examine whether transporter(s) other than CTL1 are involved in choline transport in A549 cells, we investigated the effect of HC-3 on the choline uptake by negative control and hCTL1 siRNA-treated A549 cells. CTL1 mRNA expression was decreased to about 15% of that in negative control siRNA-treated A549 cells. The choline uptake in negative control siRNA-treated A549 cells was significantly inhibited by HC-3 but that in CTL1 siRNA-treated A549 cells was hardly inhibited (Fig. 7).

Inhibitory effect of gefitinib on [^{3}H]choline transport in A549 and primary-cultured rat ATII cells. The inhibitory effect of gefitinib on the initial uptake of [^{3}H]choline was evaluated in A549 and primary-cultured rat ATII cells. Gefitinib strongly inhibited [^{3}H]choline uptake by A549 and rat ATII cells with IC_{50} values of 19.9±2.07 and 85.8±13.1 μM, respectively (Fig. 8a and b). When A549 and rat ATII cells were preincubated with various concentrations of gefitinib for 60 min, the inhibitory effect of gefitinib on the choline uptake was significantly increased, and the IC_{50} values became 6.77±0.604 and 10.5±0.728 μM, respectively (Fig. 8a and b). We assessed the interaction between gefitinib and choline uptake in A549 cells with and without preincubation of A549 cells with gefitinib. In the absence of preincubation of A549 cells with gefitinib, the plots of the choline uptake in the absence and presence of gefitinib almost intersected at the horizontal axis (Fig. 9a). On the other hand, when the cells were preincubated with gefitinib, the plots did not intersect at the horizontal axis (Fig. 9b). The kinetic parameter (Km and Vmax) values without and with preincubation are shown in Table II.

DISCUSSION

Gefitinib is an anticancer agent that acts as a selective inhibitor of EGFR-TK. Gefitinib has been associated with sudden and normal onset of severe ILD with the low incidence of 1% worldwide (19). However, the molecular mechanisms of both sudden and normal onset of ILD associated with gefitinib treatment remain largely uncharacterized.

PC is synthesized from choline within ATII epithelia and secreted into the alveolar lumen via lamellar bodies as the major phospholipid component of lung surfactant, which is essential to establish normal breathing. ABCA3 recognizes

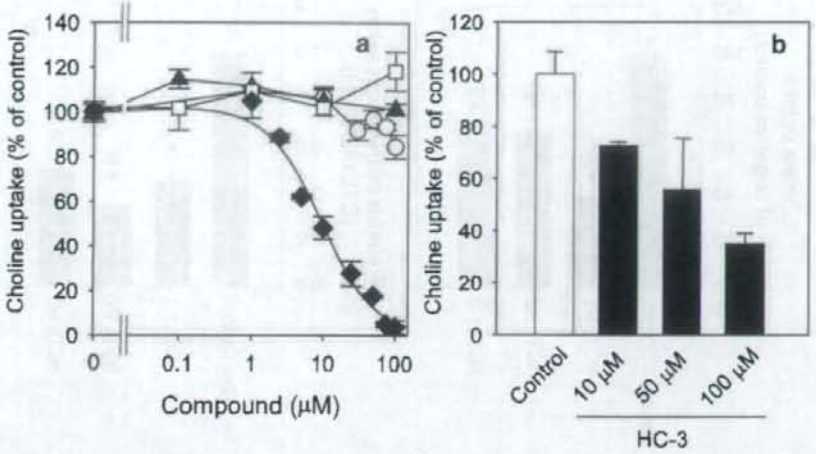

Fig. 4. Effect of various compounds on the uptake of [^{3}H]choline by A549 (**a**) and rat ATII cells (**b**). The substrate concentration was 0.1 μM. Transporter-mediated uptake of [^{3}H]choline by A549 and rat ATII cells was expressed as the difference between the uptakes at 37 and 4°C. Data are shown as percentages of the transporter-mediated uptake of [^{3}H]choline in the absence of inhibitors. *Squares*, *triangles*, *circles* and *diamonds* represent the uptake of [^{3}H]choline in the presence of histamine, corticosterone, MPP^+ and HC-3, respectively. *Solid lines* represent the fitted curves obtained by nonlinear regression analysis. Each point represents the mean ± S.E. from at least 3 wells.

PC as a substrate and transports PC into lamellar bodies in ATII cells (20,21). Mutation of ABCA3 is reported to cause neonatal respiratory distress syndrome and ILD (22), and ABCA3 knock-out mice die within an hour after birth (23). It is considered that the cause of the neonatal respiratory distress syndrome and death of the mice is the lack of secretion of PC into alveolar space due to the decreased ABCA3 activity. Furthermore, changes in PC content are significantly correlated with loss of surface activity in patients with ILD (24).

To elucidate the mechanism of ILD associated with gefitinib, we focused on lung surfactant synthesis and tested

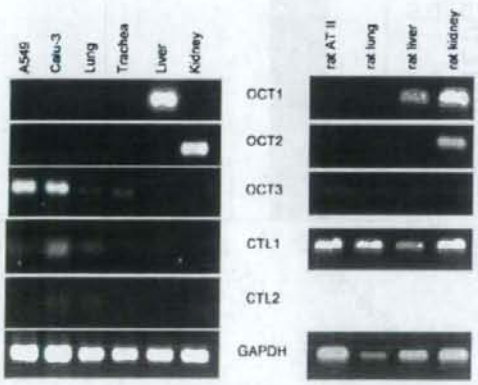

Fig. 5. Expression of several transporter mRNAs in A549 cells, Calu-3 cells, lung, trachea, liver, kidney, primary-cultured rat ATII cells, rat lung, rat liver and rat kidney. The reactions using specific primer sets were described in the text. PCR products were separated by electrophoresis in 1–1.5% agarose gel and ethidium bromide was used to visualize bands.

the hypothesis that gefitinib reduces PC biosynthesis via inhibition of cellular choline uptake, resulting in abnormality of lung surfactant. We also examined that choline transport in A549 and primary-cultured rat ATII cells, and found that it is mediated by a weakly Na^+-dependent transporter, which has transport characteristics similar to those of human and rat CTL1.

Firstly, we investigated whether gefitinib impairs the biosynthesis of PC in A549 and rat ATII cells. The apparent uptake and incorporation into PC of externally added [^{3}H]choline by A549 and rat ATII cells was markedly reduced by 20 and 50 μM gefitinib (Fig. 2b and e). Twenty and 50 μM gefitinib reduced the apparent uptake of [^{3}H]choline by A549 and rat ATII cells to about 50 and 70%, which was comparable to the values of 57.7 and 64.1% for incorporation into PC in the respective cells. These results suggested that 20 and 50 μM gefitinib may not affect three enzymes involved in the CDP-choline pathway but choline uptake. In rats, the total radioactivity related to [^{14}C]gefitinib in lung did not change greatly up to 6 h (25). To check the effect of gefitinib existing in lung for hours on the incorporation of choline into PC, we evaluated the inhibitory effects of gefitinib after a 60 min preincubation of A549 and rat ATII cells with gefitinib. The incorporation of choline into PC in A549 and rat ATII cells was more strongly inhibited by gefitinib than those in the absence of preincubation (Fig. 2c and f). The inhibitory effect was also observed on the apparent uptake of [^{3}H]choline by both cells. These observations with or without preincubation suggest that the choline uptake process largely regulates the incorporation of choline into PC in A549 and rat ATII cells.

To characterize the choline transport regulating PC biosynthesis in A549 and rat ATII cells, we performed choline uptake studies by both cells. [^{3}H]Choline was taken up into A549 cells in a time-, temperature- and concentration-

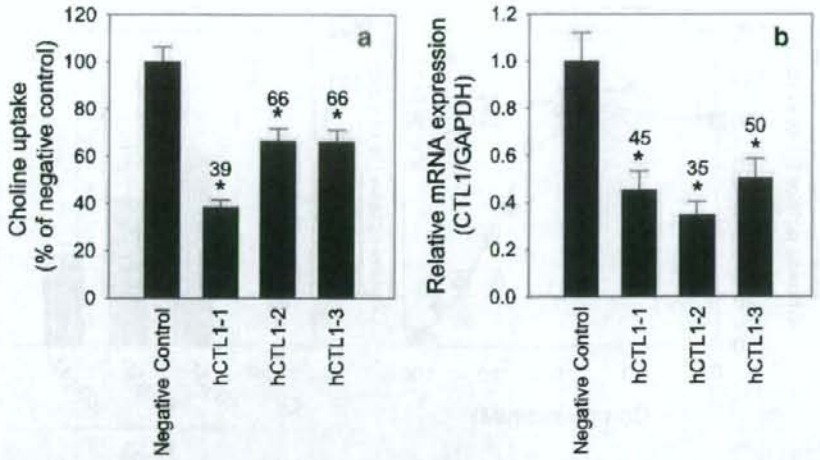

Fig. 6. Effect of hCTL1 siRNA on [^{3}H]choline uptake (**a**) and hCTL1 mRNA expression (**b**) in A549 cells. [^{3}H]Choline uptake (0.1 μM) was evaluated at 30 s. Transporter-mediated uptake of [^{3}H]choline was expressed as the difference between the uptakes at 37 and 4°C. Quantitative RT-PCR using specific primer sets were done as described in the text. The histogram shows hCTL1 mRNA knockdown data as the hCTL1/GAPDH ratio. Values above bars are percentages of choline uptake and CTL1 mRNA in the negative control siRNA-treated A549 cells. Each point represents the mean ± S.E. of at least 3 wells. * $p<0.05$ compared with the negative control siRNA.

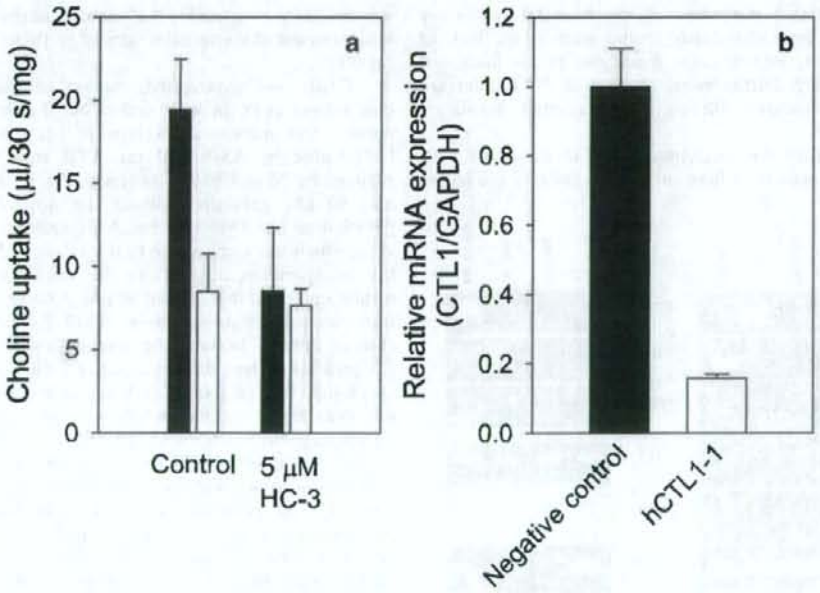

Fig. 7. Effect of HC-3 on the uptake of [^{3}H]choline by negative control siRNA- and CTL1 siRNA-treated A549 cells. The substrate concentration was 0.1 μM. **a** Transporter-mediated uptake of [^{3}H]choline by A549 cells was expressed as the difference between the uptakes at 37 and 4°C. The *filled* and *open bars* represent choline uptake by negative control and CTL1 siRNA-transfected A549 cells, respectively. **b** Quantitative RT-PCR using specific primer sets were done as described in the text. hCTL1 mRNA knockdown data was shown as the hCTL1/GAPDH ratio. Each point represents the mean ± S.E. from at least 3 wells.

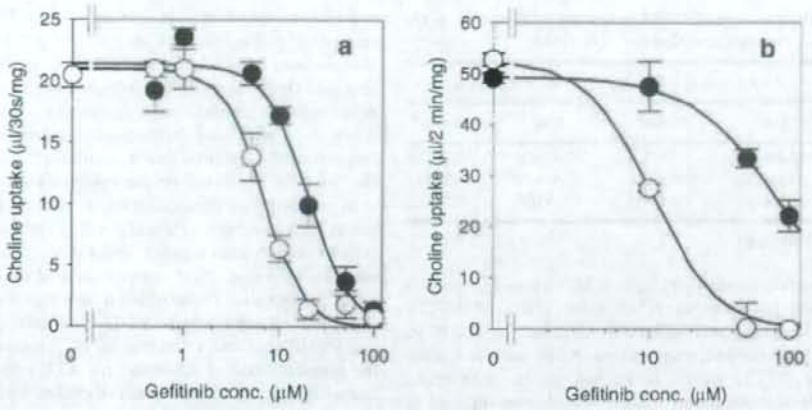

Fig. 8. Inhibitory effect of gefitinib on [^{3}H]choline uptake by A549 (**a**) and rat primary-cultured ATII cells (**b**) with or without preincubation. Transporter-mediated uptake of [^{3}H]choline was expressed as the difference between the uptakes at 37 and 4°C. *Closed* and *open circles* represent the transporter-mediated uptake of [^{3}H]choline in the absence and presence of preincubation of A549 and rat ATII cells with gefitinib, respectively. [^{3}H]Choline (0.1 μM) was incubated with various concentrations of gefitinib (0.5–100 μM for A549 cells and 10–100 μM for rat ATII cells) for 30 s and 2 min, respectively. The *solid line* represents the mean ± S.E. from at least 3 wells.

dependent manner, demonstrating that the uptake is transporter-mediated. For further characterization of [^{3}H]choline transport, the time of 30 s was used for the evaluation of initial uptake in A549 cells. The K_m value (15 μM) in A549 cells is about 10 times higher than that of CHT1 (1.6 μM) (26), and comparable to those of CTL1 and OCT2 (53–102 μM) (9,27). The uptake of [^{3}H]choline by A549 cells showed membrane potential-, pH-, and weak Na^+-dependence (Fig. 3). These transport properties of choline uptake in A549 cells are similar to those of OCTs and CTLs (27,28). A choline analogue, HC-3, reduced the choline uptake by A549 cells with the IC_{50} value of 9.48 μM, whereas corticosterone, histamine and MPP^+, which are substrates and inhibitors of OCT1, 2, and 3, were not inhibitory up to 100 μM (Fig. 4). RT-PCR analysis revealed the expression of OCT3 and CTL1 mRNAs in A549 cells (Fig. 5). Based on the results that the IC_{50} value of HC-3 for choline transport in A549 cells was much higher than that for CHT1-mediated choline transport (5 nM) (26), that OCT3 substrate and/or inhibitors did not inhibit choline uptake by A549 cells, and that OCT3 hardly recognizes choline as the substrate (9), the involvements of CHT1 and OCT3 in choline transport in the cells were considered to be negligible. The three different siRNAs targeted to the three different regions of the hCTL1 gene reduced both hCTL1 mRNA expression and choline transport activity in A549 cells to about 50%, indicating that the contribution of hCTL1 to transporter-mediated choline uptake in A549 cells is at least 50% (Fig. 7). On the basis of the

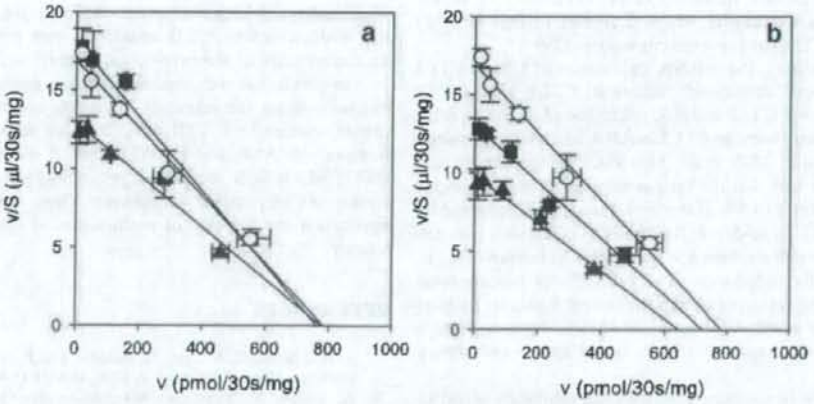

Fig. 9. Eadie–Hofstee plots of the interaction between choline and gefitinib without (**a**) or with (**b**) preincubation of A549 cells. Concentration dependent uptake of [^{3}H]choline (1–100 μM) was examined at 30 s in the absence (*circles*) or presence of 3 μM (*squares*) and 10 μM (*triangles*) gefitinib. Transporter-mediated uptake of [^{3}H]choline was expressed as the difference between the uptakes at 37 and 4°C. The *solid line* represents the fitted curve. Each point represents the mean ± S.E. from at least 3 wells.

Table II. Kinetic Parameters of Choline Uptake by A549 Cells in the Presence and Absence of Gefitinib

Gefitinib	Preincubation (−)		Preincubation (+)	
	Km[a]	Vmax[b]	Km[a]	Vmax[b]
+ 0 μM	43.4±6.54	717±61.6	43.4±6.54	717±61.6
+ 3 μM	39.1±6.37	688±70.1	52.4±6.10	681±46.9
+ 10 μM	56.2±6.48	732±53.3	70.0±10.6	650±62.3

[a] (μM), [b] (pmol/30 s/mg)

transport properties, inhibitory effects of various compounds on [^{3}H]choline transport in A549 cells, effect of hCTL1 siRNA and the transporter molecules identified by RT-PCR, we consider that choline transport in A549 cells is mainly mediated by CTL1, which is known to be membrane potential-, pH-dependent and weakly Na^+-dependent, and to have affinity for choline and HC-3 (27). In CTL1 siRNA-treated A549 cells, 5 μM HC-3, which is a concentration close to IC_{50} of HC-3 on CTL1-mediated choline transport, did not exhibit the inhibitory effect on choline uptake compared to that observed in negative control siRNA-treated A549 cells. This result indicates that CTL1 mainly contributes to the uptake of choline, while the involvement of transporter(s) other than CTL1 cannot be excluded in choline transport by A549 cells. Further experiments will be required to identify the transporter molecule(s) involved.

The mechanism of choline uptake into rat ATII cells was reported previously (29). In this study, we confirmed that the profile of choline uptake in our primary-cultured rat ATII cells was similar to that previously reported. [^{3}H]Choline was taken up by rat ATII cells time-dependently for up to 5 min. The initial uptake of choline evaluated at 2 min showed weak Na^+-dependence. The Km value of choline uptake by rat ATII cells was predicted to be 10–100 μM and the IC_{50} of HC-3 for the choline uptake by rat ATII cells was estimated to be 79.9 μM. These results are comparable with reported data (29). Furthermore, CTL1 mRNA expression in primary-cultured rat ATII cells was confirmed. Accordingly, we consider that choline transport in rat ATII cells is mainly mediated by a transporter which is similar to that in A549 cells and to CTL1, as reported previously (29).

In human lung, the mRNA expression of CTL1, CTL2 and OCT3 was confirmed, whereas CTL1 and OCT3 mRNAs, but not CTL2 mRNA, were found in A549 cells. There is a discrepancy in CTL2 mRNA expression between human lung and A549 cells. This discrepancy can be explained by the fact that the lung is composed of many types of cells, and only 2 to 5% of the alveolar space is occupied by ATII cells (30). In addition, the mRNA expression patterns of the transporters examined were similar in human and rat. Considering the occupancy of ATII cells in human lung, and the transporter expression pattern and transport properties of choline in rat ATII cells, A549 cells seem to have a similar choline transport system to intact human pulmonary ATII cells.

Finally, we further characterized the inhibitory effect of gefitinib on choline transport in A549 and rat ATII cells. Gefitinib inhibited [^{3}H]choline uptake with the IC_{50} values of 19.9 μM in A549 cells and 85.8 μM in rat ATII cells (Fig. 8). Furthermore, preincubation of A549 and rat ATII cells with gefitinib reduced the IC_{50} values to 6.77 and 10.5 μM, respectively (Fig. 8). The interaction between gefitinib and choline was kinetically studied. The Eadie–Hofstee plots revealed that the modes of inhibition of choline uptake into A549 cells by gefitinib were competitive and mixed type for A549 cells with and without preincubation with gefitinib, respectively. Gefitinib has a similar chemical structure to choline (Fig. 1). Based on the inhibitory kinetics by gefitinib with and without preincubation, it is considered that CTL1 has at least two binding sites (possibly extracellular and intracellular or intramembrane), and the concentrations at these sites are both important determinants of the inhibitory effect on CTL1 activity. Preincubation also had a similar effect on the extent of inhibition of PC biosynthesis. Accordingly, it is considered that the reduction of PC biosynthesis caused by the preincubation of A549 and rat ATII cells with gefitinib is caused largely by the reduction of choline uptake process.

The maximum plasma total concentration of gefitinib observed at a clinically relevant dose is 0.5 to 1 μM or higher, but the plasma concentration shows inter-individual variability amounting to 6- to 10-fold among patients (31–34). Considering that about 90% of gefitinib in blood is bound to plasma proteins, that the total radioactivity of gefitinib is concentrated in the lung with a ratio higher than 10, and that the total radioactivity in lung does not change greatly for up to 6 h in rats (25), the concentration of gefitinib in the lung can be estimated to be about 1 μM, and this level may be maintained in the lung for several hours. This gefitinib concentration in lung is close to the IC_{50} value of 6.77 μM obtained in the present study. When CYP3A4-mediated gefitinib metabolism, which is a major clearance pathway of gefitinib, is inhibited by the potent CYP3A4 inhibitor itraconazole, the gefitinib plasma concentration is increased (35). For cancer therapy, gefitinib will be co-administered with a range of other drugs. If the major metabolic pathway and the transport process of gefitinib are inhibited by co-administered drugs and/or altered by genetic polymorphisms of the involved enzymes and transporters, the unbound gefitinib concentration in the lung may exceed the IC_{50} value, resulting in impaired PC biosynthesis that may lead to abnormality of lung surfactant. Accordingly, it is probable that sudden onset of ILD associated with gefitinib is due to an abnormality of the production of lung surfactant.

In conclusion we demonstrated that gefitinib reduces PC biosynthesis via the inhibition of choline uptake by A549 and primary-cultured rat ATII cells. We also showed that choline transport by A549 and rat ATII cells is mainly mediated by CTL1, which is a membrane potential-, pH-dependent and weakly Na^+-dependent transporter. These results may have implication for the one of mechanisms of drug-induced lung toxicity.

REFERENCES

1. S. H. Landis, T. Murray, S. Bolden, and P. A. Wingo. Cancer statistics, 1999. *CA Cancer J. Clin.* **49**:8–31 (1999).
2. A. Inoue, Y. Saijo, M. Maemondo, K. Gomi, Y. Tokue, Y. Kimura, M. Ebina, T. Kikuchi, T. Moriya, and T. Nukiwa. Severe acute interstitial pneumonia and gefitinib. *Lancet* **361**:137–139 (2003).
3. I. Okamoto, K. Fujii, M. Matsumoto, Y. Terasaki, N. Kihara, H. Kohrogi, and M. Suga. Diffuse alveolar damage after

ZD1839 therapy in a patient with non-small cell lung cancer. *Lung Cancer* **40**:339–42 (2003).
4. N. Thatcher, A. Chang, P. Parikh, J. Rodrigues Pereira, T. Ciuleanu, J. von Pawel, S. Thongprasert, E. H. Tan, K. Pemberton, V. Archer, and K. Carroll. Gefitinib plus best supportive care in previously treated patients with refractory advanced non-small-cell lung cancer: results from a randomised, placebo-controlled, multicentre study (Iressa Survival Evaluation in Lung Cancer). *Lancet* **366**:1527–1537 (2005).
5. K. Aoe, A. Hiraki, T. Murakami, T. Maeda, Y. Umemori, H. Katayama, R. Eda, and H. Takeyama. Sudden onset of interstitial lung disease induced by gefitinib in a lung cancer patient with multiple drug allergy. *Anticancer Res.* **25**:415–418 (2005).
6. N. N. Jarjourand and G. Enhorning. Antigen-induced airway inflammation in atopic subjects generates dysfunction of pulmonary surfactant. *Am. J. Respir. Crit. Care Med.* **160**:336–341 (1999).
7. A. H. Jobeand and M. Ikegami. Surfactant and acute lung injury. *Proc. Assoc. Am. Physicians* **110**:489–495 (1998).
8. P. R. Lockmanand and D. D. Allen. The transport of choline. *Drug Dev. Ind. Pharm.* **28**:749–771 (2002).
9. D. H. Sweet, D. S. Miller, and J. B. Pritchard. Ventricular choline transport: a role for organic cation transporter 2 expressed in choroid plexus. *J. Biol. Chem.* **276**:41611–41619 (2001).
10. T. Okuda, T. Haga, Y. Kanai, H. Endou, T. Ishihara, and I. Katsura. Identification and characterization of the high-affinity choline transporter. *Nat. Neurosci.* **3**:120–125 (2000).
11. H. Misawa, K. Nakata, J. Matsuura, M. Nagao, T. Okuda, and T. Haga. Distribution of the high-affinity choline transporter in the central nervous system of the rat. *Neuroscience* **105**:87–98 (2001).
12. S. O'Regan and F. M. Meunier. Selection and characterization of the choline transport mutation suppressor from Torpedo electric lobe, CTL1. *Neurochem. Res.* **28**:551–555 (2003).
13. S. O'Regan, E. Traiffort, M. Ruat, N. Cha, D. Compaore, and F. M. Meunier. An electric lobe suppressor for a yeast choline transport mutation belongs to a new family of transporter-like proteins. *Proc. Natl. Acad. Sci. USA* **97**:1835–1840 (2000).
14. M. Lieber, B. Smith, A. Szakal, W. Nelson-Rees, and G. Todaro. A continuous tumor-cell line from a human lung carcinoma with properties of type II alveolar epithelial cells. *Int. J. Cancer.* **17**:62–70 (1976).
15. K. Miquel, A. Pradines, F. Terce, S. Selmi, and G. Favre. Competitive inhibition of choline phosphotransferase by geranylgeraniol and farnesol inhibits phosphatidylcholine synthesis and induces apoptosis in human lung adenocarcinoma A549 cells. *J. Biol. Chem.* **273**:26179–26186 (1998).
16. L. G. Dobbs, R. Gonzalez, and M. C. Williams. An improved method for isolating type II cells in high yield and purity. *Am. Rev. Respir. Dis.* **134**:141–145 (1986).
17. Y. Kikkawa and K. Yoneda. The type II epithelial cell of the lung. I. Method of isolation. *Lab. Invest.* **30**:76–84 (1974).
18. E. G. Bligh and W. J. Dyer. A rapid method of total lipid extraction and purification. *Can. J. Biochem. Physiol.* **37**:911–917 (1959).
19. M. H. Cohen, G. A. Williams, R. Sridhara, G. Chen, W. D. McGuinn, Jr., D. Morse, S. Abraham, A. Rahman, C. Liang, R. Lostritto, A. Baird, and R. Pazdur. United States Food and Drug Administration Drug Approval summary: Gefitinib (ZD1839; Iressa) tablets. *Clin. Cancer Res.* **10**:1212–1218 (2004).
20. G. Yamano, H. Funahashi, O. Kawanami, L. X. Zhao, N. Ban, Y. Uchida, T. Morohoshi, J. Ogawa, S. Shioda, and N. Inagaki. ABCA3 is a lamellar body membrane protein in human lung alveolar type II cells. *FEBS Lett.* **508**:221–225 (2001).
21. N. Cheong, M. Madesh, L. W. Gonzales, M. Zhao, K. Yu, P. L. Ballard, and H. Bullard. Functional and trafficking defects in ATP binding cassette A3 mutants associated with respiratory distress syndrome. *J. Biol. Chem.* **281**:9791–9800 (2006).
22. J. E. Bullard, S. E. Wert, and L. M. Nogee. ABCA3 deficiency: neonatal respiratory failure and interstitial lung disease. *Semin. Perinatol.* **30**:327–334 (2006).
23. N. Ban, Y. Matsumura, H. Sakai, Y. Takanezawa, M. Sasaki, H. Arai, and N. Inagaki. ABCA3 as a Lipid Transporter in Pulmonary Surfactant Biogenesis. *J. Biol. Chem.* **282**:9628–9634 (2007).
24. R. Schmidt, U. Meier, P. Markart, F. Grimminger, H. G. Velcovsky, H. Morr, W. Seeger, and A. Gunther. Altered fatty acid composition of lung surfactant phospholipids in interstitial lung disease. *Am. J. Physiol. Lung. Cell. Mol. Physiol.* **283**:L1079–L1085 (2002).
25. D. McKillop, M. Hutchison, E. A. Partridge, N. Bushby, M. Cooper, J. A. Clarkson-Jones, W. Herron, and H. C. Swaisland. Metabolic disposition of gefitinib, an epidermal growth factor receptor tyrosine kinase inhibitor, in rat, dog and man. *Xenobiotica* **34**:917–934 (2004).
26. S. Apparsundaram, S. M. Ferguson, A. L. George Jr., and R. D. Blakely. Molecular cloning of a human, hemicholinium-3-sensitive choline transporter. *Biochem. Biophys. Res. Commun.* **276**:862–867 (2000).
27. M. D. Fullerton, L. Wagner, Z. Yuan, and M. Bakovic. Impaired trafficking of choline transporter like protein-1 at the plasma membrane and inhibition of choline transport in THP-1 monocyte-derived macrophages. *Am. J. Physiol. Cell Physiol.* (2005).
28. V. Gorboulev, J. C. Ulzheimer, A. Akhoundova, I. Ulzheimer-Teuber, U. Karbach, S. Quester, C. Baumann, F. Lang, A. E. Busch, and H. Koepsell. Cloning and characterization of two human polyspecific organic cation transporters. *DNA Cell Biol.* **16**:871–881 (1997).
29. G. D. Rossumandvan and C. A. Boyd. Sodium-dependent and -independent choline uptake by type II epithelial cells from rat lung. *J. Membr. Biol.* **162**:147–156 (1998).
30. K. C. Stone, R. R. Mercer, P. Gehr, B. Stockstill, and J. D. Crapo. Allometric relationships of cell numbers and size in the mammalian lung. *Am. J. Respir. Cell Mol. Biol.* **6**:235–243 (1992).
31. J. Baselga, D. Rischin, M. Ranson, H. Calvert, E. Raymond, D. G. Kieback, S. B. Kaye, L. Gianni, A. Harris, T. Bjork, S. D. Averbuch, A. Feyereislova, H. Swaisland, F. Rojo, and J. Albanell. Phase I safety, pharmacokinetic, and pharmacodynamic trial of ZD1839, a selective oral epidermal growth factor receptor tyrosine kinase inhibitor, in patients with five selected solid tumor types. *J. Clin. Oncol.* **20**:4292–4302 (2002).
32. R. S. Herbst, A. M. Maddox, M. L. Rothenberg, E. J. Small, E. H. Rubin, J. Baselga, F. Rojo, W. K. Hong, H. Swaisland, S. D. Averbuch, J. Ochs, and P. M. LoRusso. Selective oral epidermal growth factor receptor tyrosine kinase inhibitor ZD1839 is generally well-tolerated and has activity in non-small-cell lung cancer and other solid tumors: results of a phase I trial. *J. Clin. Oncol.* **20**:3815–3825 (2002).
33. K. Nakagawa, T. Tamura, S. Negoro, S. Kudoh, N. Yamamoto, K. Takeda, H. Swaisland, I. Nakatani, M. Hirose, R. P. Dong, and M. Fukuoka. Phase I pharmacokinetic trial of the selective oral epidermal growth factor receptor tyrosine kinase inhibitor gefitinib ('Iressa', ZD1839) in Japanese patients with solid malignant tumors. *Ann. Oncol.* **14**:922–930 (2003).
34. M. Ranson, L.A. Hammond, D. Ferry, M. Kris, A. Tullo, P. I. Murray, V. Miller, S. Averbuch, J. Ochs, C. Morris, A. Feyereislova, H. Swaisland, and E. K. Rowinsky. ZD1839, a selective oral epidermal growth factor receptor-tyrosine kinase inhibitor, is well tolerated and active in patients with solid, malignant tumors: results of a phase 1 trial. *J. Clin. Oncol.* **20**:2240–2250 (2002).
35. H. C. Swaisland, M. Ranson, R. P. Smith, J. Leadbetter, A. Laight, D. McKillop, and M. J. Wild. Pharmacokinetic drug interactions of gefitinib with rifampicin, itraconazole and metoprolol. *Clin. Pharmacokinet.* **44**:1067–1081 (2005).
36. M. Hayer-Zillgen, M. Bruss, and H. Bonisch. Expression and pharmacological profile of the human organic cation transporters hOCT1, hOCT2 and hOCT3. *Br. J. Pharmacol.* **136**:829–836 (2002).
37. J. Alcorn, X. Lu, J. A. Moscow, and P. J. McNamara. Transporter gene expression in lactating and nonlactating human mammary epithelial cells using real-time reverse transcription-polymerase chain reaction. *J. Pharmacol. Exp. Ther.* **303**:487–496 (2002).
38. D. Kristufek, W. Rudorfer, C. Pifl, and S. Huck. Organic cation transporter mRNA and function in the rat superior cervical ganglion. *J. Physiol.* **543**:117–134 (2002).
39. M. Inazu, H. Takeda, and T. Matsumiya. Molecular and functional characterization of an Na+-independent choline transporter in rat astrocytes. *J. Neurochem.* **94**:1427–1437 (2005).

J Cancer Res Clin Oncol (2008) 134:1199–1206
DOI 10.1007/s00432-008-0401-7

ORIGINAL PAPER

Development and verification of a prediction model using serum tumor markers to predict the response to chemotherapy of patients with metastatic or recurrent breast cancer

Kan Yonemori · Noriyuki Katsumata · Ayako Noda · Hajime Uno · Mayu Yunokawa · Eriko Nakano · Tsutomu Kouno · Chikako Shimizu · Masashi Ando · Kenji Tamura · Masahiro Takeuchi · Yasuhiro Fujiwara

Received: 4 February 2008 / Accepted: 21 April 2008 / Published online: 5 June 2008

Abstract
Purpose The aim of this study was to develop a prediction model using serum tumor markers to predict the response to chemotherapy of patients with metastatic or recurrent breast cancer.
Methods We retrospectively analyzed a training set of 105 patients with metastatic or recurrent breast cancer. Their chemotherapeutic response had been evaluated according to the World Health Organization (WHO)'s response criteria. Our model for predicting response using carcinoembryonic antigen (CEA), carbohydrate antigen (CA) 15-3, and NCC-ST-439 was determined using the area under the receiver operating characteristic curve (ROC-AUC) and the overall misclassification rate (OMR) in a random cross-validation. The prediction model was then verified in a consecutive set of 64 patients. Their response had been evaluated using the response evaluation criteria in solid tumors (RECIST) criteria.
Results The best prediction model consisted of the serum CEA, CA15-3, and NCC-ST-439 levels, but the prediction formula varied according to the baseline CA15-3 level (elevated or normal). The overall ROC-AUC and OMR in the training set were 0.83 and 0.19, respectively. The overall ROC-AUC and OMR in the verification set were 0.72 and 0.28, respectively. When the verification set was stratified according to either the objective response or the predicted response, the time-to-progression, but not the overall survival, was significantly different.
Conclusion Our model for predicting the response to first-line chemotherapy of patients with metastatic or recurrent breast cancer may be valid because it predicted the outcome of more than 70% of the patients in an independent verification set.

Keywords Tumor marker · Response · Prediction · Breast cancer · Chemotherapy

Introduction

Breast cancer remains the major cause of death from cancer among woman throughout the world. Most patients with metastatic or recurrent breast cancer receive chemotherapy with a palliative intent. Presently, anthracylines (doxorubicin, epirubicin) and taxanes (docetaxel, paclitaxel) are two of the most effective anticancer drugs against breast cancer (Veronesi et al. 2005). Breast cancer is generally monitored, and the response to chemotherapy is evaluated according to standardized response criteria that are based on changes in the size of measurable disease (World Health Organization 1979; Therasse et al. 2000). Response to chemotherapy confers symptom relief for patients and resolves the visceral crisis. A patient's initial response to chemotherapy is also an important source of information when deciding whether to continue chemotherapy in individual patients.

Breast cancer frequently metastasizes, and metastases can be found in almost every organ, including bone, lung,

K. Yonemori (✉) · N. Katsumata · M. Yunokawa · E. Nakano · T. Kouno · C. Shimizu · M. Ando · K. Tamura · Y. Fujiwara
Breast and Medical Oncology Division,
National Cancer Center Hospital, 5-1-1 Tsukiji,
Chuo-ku, Tokyo 104-0045, Japan
e-mail: kyonemor@ncc.go.jp

A. Noda · H. Uno · M. Takeuchi
Division of Biostatistics, School of Pharmaceutical Sciences,
Kitasato University, 5-9-1, Shirokane, Minato-ku, Tokyo, Japan

pleura, liver, lymph nodes, soft-tissue, and the brain. Two-thirds of patients with recurrent breast cancer present with distant metastasis, usually in a single organ. The most common sites of disease at the time of first recurrence are the bone, lung, and liver (Wood et al. 2004). Therefore, physicians frequently face problems deciding whether to administer chemotherapy to patients with only non-measurable diseases, such as bone metastases, malignant effusions, or lymphangitis carcinomatosa.

For many malignancies, serum tumor markers play an important role in patient management. Serum tumor markers can potentially be used for cancer screening, aiding diagnosis, determining both risk groups and prognosis, surveillance after primary surgery, monitoring treatment, and predicting response. Many serum tumor markers have been investigated in patients with breast cancer, including carcinoembryonic antigen (CEA), carbohydrate antigen (CA) 15-3, CA 549, CA 27.29, NCC-ST-439, tissue polypeptide antigen, tissue polypeptide specific antigen, and the extracellular form of HER2 (Duffy 2001, 2006). Despite numerous investigations; however, the roles of serum tumor markers have not yet been established in patients with breast cancer. Therefore, the routine measurement of serum tumor markers in patients with metastatic breast cancer is not recommended in the clinical guidelines of the American Society of Clinical Oncology, at present (Harris et al. 2007).

Predicting chemotherapeutic responses is challenging. We suspected that serum tumor markers might be useful in predicting patient response to chemotherapy. The development of an appropriate prediction model would contribute to treatment monitoring and the decision-making process, particularly when an objective response has not been observed during early courses of chemotherapy or in patients with no measurable disease. The aim of this study was to develop a prediction model using serum tumor markers to predict the response to first-line chemotherapy in patients with metastatic or recurrent breast cancer, and to evaluate the predictive accuracy of the resulting prediction model in a consecutive validation set.

Patients and methods

Patients in the training set

Between January 1999 and May 2003, a total of 105 consecutive patients with metastatic or recurrent breast cancer (the training set) were enrolled in a multi-center phase III trial for first-line chemotherapy at the National Cancer Center Hospital (Katsumata et al. 2005). The patients were randomized into three groups: six courses of AC therapy (doxorubicin (A), 40 mg/m^2, day 1; cyclophosphamide (C) 500 mg/m^2, day 1, q3w), six courses of docetaxel therapy (docetaxel, 60 mg/m^2, q3w), or three courses of alternating AC therapy and docetaxel therapy. Trastuzumab combination therapy was not available for patients with metastatic or breast cancer during the enrollment period of this study. The primary endpoint was the time-to-treatment-failure of the first-line chemotherapy. For the purpose of the present study, we retrieved the clinical records of 105 patients with measurable lesions whose response to chemotherapy had been prospectively assessed in the phase III trial. After every 2 courses of chemotherapy, routine evaluations of the treatment responses of measurable lesions were performed according to the WHO criteria; these evaluations included clinical examinations, chest radiography, computed tomography, and skeletal radiography or bone scanning, when necessary (World Health Organization 1979). The patients signed a written informed consent form approved by the institutional review board for use in clinical trials and agreeing to the review of records and images for research purposes.

Serum tumor marker measurements

In all the patients in the present study, a complete blood cell count, chemistry and serum tumor markers were measured using blood samples obtained within 1 week of the start of chemotherapy and obtained on day 1 of every course of chemotherapy administration to avoid cytolytic effects; the samples were immediately assayed in the laboratory division of the National Cancer Center Hospital. The serum CEA and CA 15-3 values were measured using chemiluminescent enzyme immunoassays (sandwich principle) with commercially available kits: lumipalse CEA-N and lumipalse CA 15-3 (both Fujirebio Diagnostics Inc., Malvern, PA, USA). Serum NCC-ST-439 values were measured using an enzyme immunoassay (sandwich principle) with a commercially available kit (Lanazyme ST-439 plate; Nippon Kayaku Co., Tokyo, Japan). Quality control and calibration for all the tumor marker measurements were strictly performed using commercial reference control sera. The coefficients of intra- and inter-assay variability for all the tumor markers were less than 10%. The upper normal limits for the CEA and CA 15-3 levels were 5 ng/mL and 28 U/mL, respectively; the upper normal limit for NCC-ST-439 was 7.0 U/mL in pre-menopausal women and 4.5 U/mL in menopausal woman. Throughout the phase III trial and clinical practice, changes in the tumor marker values never influenced the treatment decision-making process.

Development of prediction model

To develop a prediction model, the documented response and the three serum tumor markers levels in the training set

were collected from the patients' medical charts as follows: baseline values, serum tumor marker values on day 1 the second chemotherapy course, and serum tumor marker values on day 1 of the third chemotherapy course. The percent changes in the serum tumor marker values were expressed according to the following formulas: MARKER (I) = (Marker value on day 1 of the second chemotherapy course − Initial marker value)/Initial marker value, MARKER (II) = (Marker value on day 1 of the third chemotherapy course − Initial marker value)/Initial marker value, and MARKER (I and II) = (Marker value on day 1 of the third chemotherapy course − Marker value on day 1 of the second chemotherapy course)/Marker value on day 1 of the second chemotherapy course.

Multivariate logistic regression models were used to derive a prediction model for the response. Several linear combinations of marker values were fitted to the entire training set. In addition, the training set was split into two subgroups and several and different combinations of markers were fitted to each subgroup, which enlarged the class of candidate prediction models. As a measure of accuracy, the area under the receiver operating characteristic curve (ROC-AUC) and the overall misclassification rate (OMR) were calculated for each candidate prediction model.

In order to reduce the bias in estimating the ROC-AUC and OMR of each prediction model, random cross-validation estimates were calculated in which a randomly selected 4/5 of training set was used to estimate the model parameter and the remaining 1/5 was used to calculate the ROC-AUC and OMR. This procedure was repeated 200 times. The best prediction model was determined by the maximum ROC-AUC. If several models with the same ROC-AUC were obtained, the model with the more parsimonious and lower OMR values was regarded as the better model.

Verification of prediction model

After the development of the prediction model, the model was verified using an independent consecutive series of 64 patients with metastatic or recurrent breast cancer who had received first-line chemotherapy in a practical setting at the National Cancer Center Hospital between January 2004 and January 2005. All the patients had adequate bone marrow and organ function. The patients had been treated with AC therapy, docetaxel therapy, or weekly paclitaxel therapy (80 mg/m^2) consisting of 3 weekly cycles followed by a week of rest. Trastuzumab combination therapy was also administered with the docetaxel or weekly paclitaxel therapy if the patient had a positive HER2 status. The responses of all the patients to chemotherapy were evaluated according to the RECIST criteria (Therasse et al. 2000). The treatment regimens were decided according to the patients' preferences. The patients signed a written informed consent form approved by the institutional review board for the review of records and images for research purposes. The ROC-AUC and OMR for the verification set were examined to evaluate the performance of the prediction model. Time-to-progression (TTP) and the overall survival (OS) time were statistically compared between the patients with and those without a predicted response according to the prediction model. TTP was measured from the first day of chemotherapy until disease progression or the final day of follow up, and OS was measured from the first day of chemotherapy until death or the final day of follow up. All statistical analyses were performed using SAS version 9.1 (SAS Institute, Cary NC, USA).

Results

Characteristics of patients in the training set

The clinical characteristics of the patients in the training set are presented in Table 1. In the training set at baseline, elevated CEA levels were observed in 39 patients (37%), elevated CA15-3 levels were observed in 49 patients (47%), and elevated NCC-ST-439 levels were observed in 44 patients (42%; 12 premenopausal women and 32 postmenopausal women). Thirty-four patients had received AC therapy, 37 patients had received docetaxel therapy, and 34 patients had received alternating AC and docetaxel therapy as their first-line chemotherapy regimen. The median number of chemotherapy courses was 6 (range 2–6). The overall response rate of the patients in the training set was 45% (95% confidence interval [CI]: 36–55%; 6 complete responses [CRs], 41 partial responses [PRs], 49 no changes [NCs], and 9 progressive diseases [PDs]). The median TTP and OS were 7.1 and 30.9 months, respectively.

Development of the prediction model

Single tumor marker at one measurement point

The ROC-AUCs of single tumor markers (CEA, CA 15-3, and NCC-ST-439) at each measurement point are shown in Table 2. The ROC-AUC of CA 15-3 at each measurement point was higher than those of CEA or NCC-ST-439, and the ROC-AUCs of the serum tumor marker values on day 1 of the third chemotherapy course were higher than other measurements points in each tumor marker. However, all ROC-AUCs were less than 0.7.

Table 1 Characteristics of patients in the training and verification sets

	Training set (%)	Verification set (%)	*P* value*
No. of patients	105	64	
Median age (range)	56 (34–76)	55 (35–76)	0.69
Diseases			
Metastatic	20 (19%)	14 (22%)	0.66
Recurrent	85 (81%)	50 (78%)	
Menopause			
Pre-menopause	30 (29%)	25 (39%)	0.16
Menopause	75 (71%)	39 (61%)	
Performance status			
0	69 (66%)	29 (45%)	0.01
0<	36 (34%)	35 (55%)	
Hormone status			
Positive	50 (48%)	41 (64%)	0.04
Negative	55 (52%)	23 (36%)	
HER2 status			
Positive	22 (21%)	20 (31%)	0.13
Negative	83 (79%)	44 (69%)	
Number of disease sites			
1–2	70 (67%)	39 (61%)	0.45
2<	35 (33%)	25 (39%)	
Site of disease			
Primary tumor	20 (19%)	15 (23%)	0.5
Lymph node	53 (50%)	30 (45%)	0.83
Lung	36 (34%)	28 (44%)	0.22
Bone	28 (27%)	29 (45%)	0.01
Liver	22 (21%)	27 (42%)	0.01

* Univariate analysis: Chi-square test and *t* tests were performed for proportional differences or mean differences between the training and verification sets (2-sided)

Combination of tumor markers (single, double or triple) and various measurement points

In the logarithmic transformation of the tumor marker values, the candidate prediction model was derived using the CA 15-3 values at baseline, day 1 of the 2nd course and day 1 of the 3rd course, and the ROC-AUC and OMR for a random cross-validation using the training set were 0.655 and 0.369, respectively. In the %changes of the serum tumor markers, the candidate prediction model using both CA 15-3 and NCC-ST-439 at baseline, day 1 of the 2nd course and day 1 of the 3rd course was derived, and the ROC-AUC and OMR for a random cross-validation using the training set were 0.636 and 0.371, respectively. From these analyses, the combination of tumor markers and measurement points improved the ROC-AUCs, and CA 15-3 had a relatively strong association compared with both CEA and NCC-ST-439. However, the ROC-AUCs of these candidate models were less than 0.7. Therefore, CA 15-3 was selected for consideration of the candidate prediction models by the condition of the serum tumor markers (such as an elevated or normal range at baseline).

Table 2 ROC-AUCs of serum tumor markers in each measurement point

Marker	Point	ROC-AUC
CEA	Baseline	0.599
	Day 1 of 2nd course	0.617
	Day 1 of 3rd course	0.639
CA 15-3	Baseline	0.631
	Day 1 of 2nd course	0.657
	Day 1 of 3rd course	0.693
NCC-ST-439	Baseline	0.580
	Day 1 of 2nd course	0.565
	Day 1 of 3rd course	0.620

The best prediction model in the present study

The candidate prediction models, taking the condition of the CA 15-3 baseline into consideration, were analyzed in both the logarithmic transformation of the tumor marker values and the %changes of the serum tumor markers. The best prediction model developed in the present study defined the probability of response as follows: probability of response = $e^x/(1 + e^x)$, where e is the base of the natural logarithm; if the baseline CA15-3 level was elevated, $x = (1.448 + 0.086 \times \text{CA15-3(I)} + 4.365 \times \text{CA15-3(II)} - 5.099 \times \text{NCC-ST439(I)} + 2.266 \times \text{NCC-ST439(II)})$, whereas if the baseline CA15-3 level was within the normal range, $x = (-0.577 - 2.683 \times \text{CEA(I)} + 3.729 \times \text{CEA (II)} + 0.504 \times \text{NCC-ST-439(I)} + 1.492 \times \text{NCC-ST-439(II)})$. The prediction rule was as follows: a calculated probability of a response ≥ 0.778 corresponded to a CR or PR, while a calculated probability of response <0.778 corresponded to a SD or PD. The ROC-AUCs of the training set were 0.86 and 0.75 (elevated and normal ranges of CA 15-3, respectively). The OMRs of the training set were 0.16 and 0.27 (elevated and normal ranges of CA 15-3, respectively). The ROC-AUCs for a random cross-validation using the training set were 0.83, and 0.64 (elevated and normal ranges of CA 15-3, respectively). The OMRs in a random cross-validation using the training set were 0.22 and 0.27 (elevated and normal ranges of CA 15-3, respectively). The overall ROC-AUC and OMR in the training set were 0.83, and 0.19, respectively (Fig. 1, point estimate).

The prediction model was influenced by the baseline level of CA 15-3; therefore, the performance of the prediction model was evaluated by changing the CA 15-3 cut-off level to every 1 U/mL between 24 and 30 U/mL (the kit

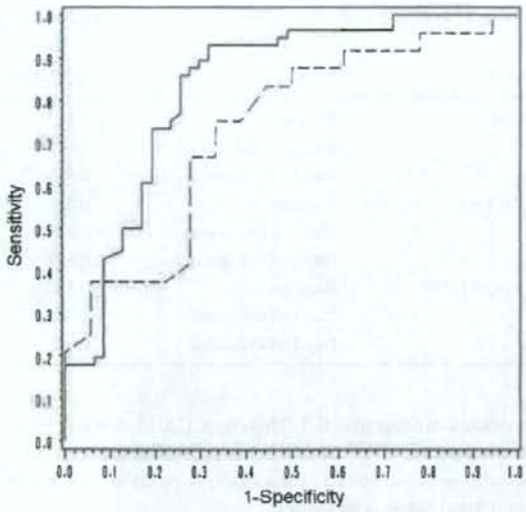

Fig. 1 Receiver operating characteristics (ROC) curve for the prediction model in the training set (*solid line*). The model was developed based on data from 104 patients with metastatic or recurrent breast cancer, who participated in a phase III trial. ROC curve for the prediction model in the verification set (*dotted line*). The verification set included 64 consecutive patients with metastatic or recurrent breast cancer

standard defined the upper normal limit as 28 U/mL). The differences in the 95% CIs for each ROC-AUC or OMR were calculated using the bootstrap method (iteration: 1,000). The ROC-AUCs and OMRs for cut-off levels of 26 or 27 U/mL were similar to that of the standard CA 15-3 cut-off level. When a cut-off level of about 25 U/mL was used, the accuracy of the prediction model for CA 15-3 within the normal limit group increased; however, the overall ROC-AUC and OMR of the prediction model were inferior to those obtained when the standard CA 15-3 cut-off level was used (point estimate), while the differences in the 95% CIs for each ROC-AUC or OMR were similar. The accuracy of the prediction model for the elevated CA 15-3 group increased, while the accuracy of the prediction model for the normal CA 15-3 group decreased when a cut-off level of about 24 U/mL was used. The accuracy of the prediction model for the elevated CA 15-3 group decreased, while the accuracy of the prediction model for the normal CA 15-3 group increased when a cut-off level of more than 28 U/mL was used. We concluded that the cut-off level defined as the kit standard was appropriate for use with the present prediction model.

Verification of the prediction model

After deriving the prediction model, an independent consecutive series of 64 patients were analyzed to verify the prediction model. Statistical differences in the patient characteristics of the training and validation sets are presented in Table 1. The median performance status and the frequency of a hormone-positive status were significantly different between the training and verification sets. The median performance status (range) in the training and verification sets were 0 (0–2) and 1 (0–2), respectively.

In the independent verification set at baseline, elevated CEA levels were observed in 45 patients (70%), elevated CA15-3 levels were observed in 42 patients (66%), and elevated NCC-ST-439 levels were observed in 36 patients (56%, 16 premenopausal women and 20 postmenopausal women). Thirty-two patients had received AC therapy, 12 patients had received docetaxel therapy, and 20 patients had received weekly paclitaxel therapy as their first-line chemotherapy regimen. Of these patients, 18 (28%) received trastuzumab in combination with their chemotherapy regimen. The median number of chemotherapy courses was 6 (range 2–6). The overall response rate of the verification set was 64% (95% CI: 52 to 76%; 4 CR, 37 PR, 15 SD, and 8 PD). The median TTP and OS were 8.0 and 22.9 months, respectively.

The overall ROC-AUC and OMR in the verification set were 0.72 and 0.28, respectively (Fig. 1, point estimate). Therefore, the prediction model probably predicted the objective response of more than 70% of the patients in a practical setting. The TTP of the verification set was statistically significant according to a log-rank test when the groups were stratified according to both the RECIST criteria and the prediction model (Fig. 2). The OS of the verification set was not statistically significant according to a log-rank test when the groups were stratified according to both the RECIST criteria and the prediction model (Fig. 3).

Discussion

This study evaluated the use of a prediction model based on three serum tumor markers for predicting the response to chemotherapy in patients with metastatic or recurrent breast cancer. Although some disparity in the patient characteristics existed between the training set and the verification set, the accuracy of the prediction model was reliable in an independent verification set using a consecutive series of patients.

The present study examined a prediction model based on the serum levels of CA 19-9, CEA, and NCC-ST-439; these tumor markers are widely measured parameters in Europe and Japan (Duffy 2006; Kurebayashi et al. 2003). CA15-3 is a serum-based product of the MUC1 gene and is the most widely used serum marker for breast cancer (Duffy 2001). CEA is a well-known serum tumor marker for a wide range of malignancies, including breast cancer. NCC-ST-439

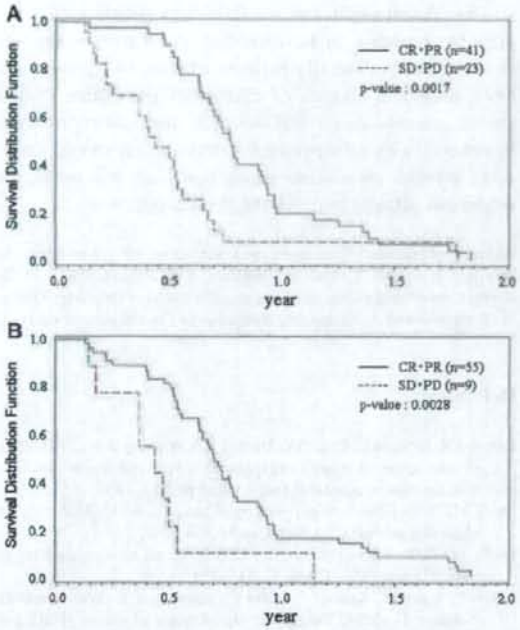

Fig. 2 Kaplan–Meier analysis of time-to-progression in the verification set. The vertical bars indicate censored cases. **a** Time-to-progression in groups stratified according to the RECIST criteria. The *dotted line* indicates patients who achieved a CR or a PR, and the *solid line* indicates patients with SD or PD. **b** Time-to-progression in groups stratified according to the prediction model. The *dotted line* indicates patients who achieved a CR or a PR, and the *solid line* indicates patients with SD or PD according to the prediction model

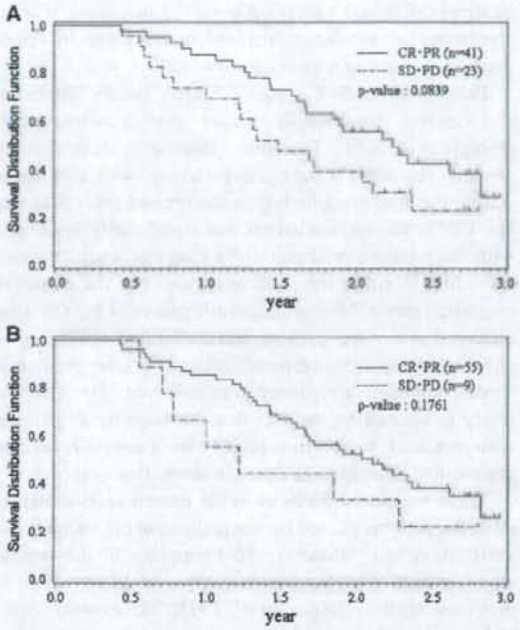

Fig. 3 Kaplan–Meier analysis of overall survival in the verification set. The *vertical bars* indicate censored cases. **a** Overall survival time in groups stratified according to the RECIST criteria. The *dotted line* indicates patients who achieved a CR or a PR, and the solid line indicates patients with SD or PD. **b** Overall survival time in groups stratified according to the prediction model. The *dotted line* indicates patients who achieved a CR or a PR, and the *solid line* indicates patients with SD or PD according to the prediction model

antigen is a tumor-related carbohydrate antigen that is recognized by a monoclonal antibody and has been shown to be elevated in gastric, colon, pancreatic and breast carcinoma (Hirohashi et al. 1984). Since serum NCC-ST439 levels are not correlated with serum CA 15-3 or CEA levels, combination assays using these tumor markers are thought to be useful in the treatment of patients with breast cancer (Narita et al. 1993).

Biological predictive and prognostic factors such as hormone receptors or HER2 have been established in breast cancer; however, this approach requires tumor tissue and is difficult to use for monitoring the response to therapy. Serum tumor markers are circulating tumor-derived molecules and biologically become surrogate markers for the tumor load. Some studies reported serum tumor markers, especially in CEA and CA 15-3, correlated with poor prognosis in breast cancer (Fehm et al. 2004; Finek et al. 2007; Hu et al. 2002). And many studies have reported that patients who respond to chemotherapy also have reduced tumor marker levels, while those with progressive disease have elevated levels. Several studies have compared serum tumor markers with objective response according to the International Unit against Cancer Criteria, providing objective data to guide therapeutic decision-making (Dixon et al. 1993; Robertson et al. 1991; Robertson et al. 1999; Van Dalen et al. 1996; Williams et al. 1990). Tampellini et al. described a general correlation between clinical response and the serum CA15-3 response in about 50–60% of patients (Tampellini et al. 2006). Therefore, the European group for serum tumor markers in breast cancer recommended that serum tumor markers should be measured prior to every chemotherapy course (Molina et al. 2005). The present study is the first to develop a prediction model based on a statistical methodology and to validate the model using an independent consecutive series. Several studies have described that an association with response was only observed in pretreatment marker-positive patients (Kurebayashi et al. 2003, 2004) While the accuracy of the prediction model for patients with abnormally elevated serum tumor markers was clearly validated, the prediction model was fairly reliable for all of the patients. While the present study contributes important information to the

treatment of breast cancer patients, the definition of what constitutes a significant increase or decrease in tumor markers is likely to remain controversial.

Patients responding to chemotherapy usually fare better and survive significantly longer than non-responders (Piergia et al. 2001). Therefore, response to chemotherapy can be considered a surrogate parameter with a dynamic status. The important finding in the present study was that the TTP in the verification set was significantly associated with the presence or absence of a response when stratified according to either the prediction model or the objective response criteria. No significant differences in the OS were observed when the patients were stratified according to either the objective response criteria or the prediction model, although a tendency was observed. The OS was likely influenced by the fact that the majority of patients with metastatic or recurrent breast cancer generally receive second-line or additional systemic chemotherapies.

There were no differences in the examination strategies or in the patterns of care for the patients in the training and verification sets. However, the limitations of the present study include a potential patient bias, similar to those in previous studies (Dixon et al. 1993; Malinowski 2007; Robertson et al. 1991; Robertson et al. 1999; Tampellini et al. 2006; Van Dalen et al. 1996). Variations in the patient population potentially exist in individual institutions over time. Furthermore, general differences in the positive rates for each tumor marker were observed. How these differences may affect the performance of the prediction model in a more generalized population is uncertain. Serum tumor markers based on tumor biology are unlikely to be influenced strongly by individual patients or institutions. However, we could not assess the accuracy of the prediction model for patients in other institutions or countries. In addition, the present study did not assess the cost-effectiveness of measuring serum biological markers; this matter will be investigated in future studies.

Radiological examinations, like computed tomography or magnetic resonance imaging, are recommended for the assessment of objective responses based on the RECIST criteria in clinical trials. However, radiological examinations for response analysis are not strictly required in practical settings. Therefore, our prediction model might reduce the need for radiological examinations and patient workups as well as the overall cost of treatment. Currently, investigators are working to develop molecular diagnostic application systems, such as genomic and proteomic profiles, for predicting the response to chemotherapy of patients with breast cancer (Malinowski 2007). These diagnostic systems continue to evolve and are not yet universally used, but they do have the potential to predict response and to improve treatment management by enabling customized therapies in the future.

The present prediction model would enable a patient's probable response to be identified at an early stage and could be used to identify patients who are likely to benefit from additional courses of chemotherapy. Future studies should evaluate the clinical utility of this prediction model in patients with non-measurable lesions and should determine whether clinical decisions based on this prediction model can actually improve the clinical outcome.

Acknowledgments This study was supported by grants from the Ministry of Health, Labor, and Welfare. The authors thanks to the Breast Cancer Study Group of Japanese Cooperative Oncology Group. K. Yonemori and A. Noda contributed equally to the present study.

References

Dixon AR, Jackson L, Chan SY, Badley RA, Blamey RW (1993) Continuous chemotherapy in responsive metastatic breast cancer: a role for tumour markers? Br J Cancer 68:181–185

Duffy MJ (2001) Biochemical markers in breast cancer: which ones are clinically useful? Clin Biochem 34:347–352

Duffy MJ (2006) Serum tumor markers in breast cancer: are they of clinical value? Clin Chem 52:345–351

Fehm T, Jagar W, Kramer S, Sohn C, Solomayer E, Wallwiener D, Gebauer G (2004) Prognostic significance of serum HER2 and CA 15-3 at the time of diagnosis of metastatic breast cancer. Anticancer Res 24:1987–1992

Finek J, Holubec L Jr, Topolcan O, Elgrova L, Skalova A, Pecen L (2007) The importance of prognostic factors in premenopausal woman with breast cancer. Anticancer Res 27:1893–1896

Harris L, Fritsche H, Mennel R, Norton L, Ravdin P, Taube S, Somerfield MR, Hayes DF, Bast RC Jr (2007) 2007 update of recommendations for the use of tumor markers in breast cancer. J Clin Oncol 33:1–26

Hirohashi S, Watanabe M, Shimosato Y, Sekine T (1984) Monoclonal antibody reactive with the sialyl-sugar residue of a high molecular weight glycoprotein in sera of cancer patients. Jpn J Cancer Res 75:485–488

Hu XC, Day W, Jones B, Loo WT, Chow LW (2002) Coparison of TPS with CEA and CA 15-3 in follow-up of Chinese breast cancer patients. Anticancer Res 22:1865–1868

Katsumata N, Minami H, Aogi K, Tabei T, Sano M, Masuda N, Andoh J, Ikeda T, Ishizuka N, Takashima S (2005) Phase III trial of doxorubicin (A)/cyclophosphamide, docetaxel(D), and alternating AC and D as front-line chemotherapy for metastatic breast cancer (MBC): Japan Clinical Oncology Group Trial (JCOG9802). Proc Am Soc Clin Oncol 23:521

Kurebayashi J, Yamamoto Y, Tanaka K, Tabei T, Sano M, Masuda N, Andoh J, Ikeda T, Ishizuka N, Takashima S (2003) Significance of carcinoembryonic antigen and CA15-3 in monitoring advanced breast cancer patients treated with systemic therapy: a large-scale retrospective study. Breast Cancer 10:38–44

Kurebayashi J, Nihimura R, Tanaka K, Kohno N, Kurosumi M, Moriya T, Ogawa Y, Taguchi T (2004) Significance of serum tumor markers in monitoring advanced breast cancer patients treated with systemic therapy: a prospective study. Breast Cancer 11:389–395

Malinowski DP (2007) Multiple biomarkers in molecular oncology. II. Molecular diagnostics application in breast cancer management. Expert Rev Mol Diag 7:269–280

Molina S, Barak V, Van Dalen A, Duffy MJ, Einarsson R, Gion M, Goike H, Lamerz R, Nap M, Soletormos G, Stieber P (2005)

Tumor markers in breast cancer-European group on tumor markers recommendations. Tumor Biol 26:281–293

Narita T, Funahashi H, Satoh Y, Imai T, Takagi H (1993) Serum and immunohistochemical studies of NCC-ST-439 in breast cancer. J Surg Oncol 54:5–8

Piergia JY, Robain M, Jouve M, Asselain B, Dieras V, Beuzeboc P, Palangie T, Dorval T, Extra JM, Scho S, Pouillart T (2001) Response to chemotherapy is a major parameter-influencing long-term survival of metastatic breast cancer patients. Ann Oncol 12:231–237

Robertson JFR, Pearson D, Price MR, Selby C, Blamey RW, Howell A (1991) Objective measurement of therapeutic response in breast cancer using tumour markers. Br J Cancer 64:757–763

Robertson JFR, Jaeger W, Syzmendera JJ, Selby C, Coleman R, Howell A, Winstanley J, Jonssen PE, Bombardieri E, Sainsbury JRC, Gronberg H, Kumpulainen E, Blamey RW (1999) The objective measurement of remission and progression in metastatic breast cancer by use of serum tumour markers. Eur J Cancer 35:47–53

Tampellini M, Berruti A, Bistossi R, Gorzegno G, Alabiso I, Bottini A, Farris A, Donadio M, Giuseppa Sarobba M, Manzin E, Durando A, Dafabiani E, De Matteis A, Ardine M, Castignlione F, Danese S, Bertone E, Alabiso O, Massobrio M, Dogliotti L (2006) Prognostic significance of changes in CA15–3 serum levels during chemotherapy in metastatic breast cancer patients. Breast Cancer Res Treat 98:241–248

Therasse P, Arbuck SG, Eisenhauer EA, Wanders J, Kaplan RS, Rubinstein L, Verweij J, Van Glabbeke M, van Oosterom AT, Chistian MC, Gwyther SG (2000) New guidelines to evaluate the response to treatment in solid tumors. European Organization for Research and Treatment of Cancer, National Cancer Institute of the United States, National Cancer Institute of Canada. J Natl Cancer Inst 92:205–216

Van Dalen A, Heering KJ, Barak V, Peretz T, Cremaschi A, Geroni P, Gion M, Saracchini S, Molina R, Namer M, Stieber P, Sturgeon C, Leonard RCF, Einarsson R (1996) Treatment response in metastatic breast cancer. Multicentre study comparing UICC criteria and tumour marker changes. Breast 5:82–88

Veronesi U, Boyle P, Goldhirsch A, Orecchia R, Viale G (2005) Breast cancer. Lancet 365:1727–1741

Williams MR, Turkes A, Pearson D, Griffiths K, Blamey RW (1990) An objective biochemical assessment of therapeutic response in metastatic breast cancer: a study with external review of clinical date. Br J Cancer 61:126–132

Wood WC, Muss HB, Solin LJ, Olopade OI (2004) Malignant tumors of the breast. In: Devita VT, Hellman S, Rosenberg SA (eds) Cancer: principle and practice of oncology. Lippincott Williams and Wilkins, Philadelphia, pp 1415–1477

World Health Organization (1979) WHO Handbook for reporting result of cancer treatment: offset publication 48. World Health Organization, Genova

Circ J 2008; **72:** 1136–1141

Dilatation of Bronchial Arteries Correlates With Extent of Central Disease in Patients With Chronic Thromboembolic Pulmonary Hypertension

Hidefumi Shimizu, MD; Nobuhiro Tanabe, MD; Jiro Terada, MD; Masahisa Masuda, MD*; Seiichiro Sakao, MD; Yasunori Kasahara, MD; Yuichi Takiguchi, MD; Koichiro Tatsumi, MD; Takayuki Kuriyama, MD

Background Dilatation of the bronchial arteries is a well-recognized feature in patients with chronic thromboembolic pulmonary hypertension (CTEPH). The purpose of the current study was to use computed tomography (CT) to assess the relationship between dilated bronchial arteries and the extent of thrombi, and to evaluate the predictive value of the former for surgical outcome.

Methods and Results Fifty-nine patients with CTEPH and 16 with pulmonary arterial hypertension (PAH) were retrospectively evaluated. The total cross-sectional area of bronchial arteries was measured by CT and its relationship with the central extent of thrombi or surgical outcome was assessed. The total area of the bronchial arteries in CTEPH patients was significantly larger than that in PAH patients (median [range], 6.9 [1.7–29.5] mm^2 vs 3.2 [0.8–9.4] mm^2), with the total area of bronchial arteries correlating with the central extent of thrombi. In patients who had undergone pulmonary thromboendarterectomy (PTE) (n=22), the change in PaO_2 after surgery had a tendency to correlate with the total area of the bronchial arteries.

Conclusion The total cross-sectional area of the bronchial arteries correlated with the extent of central disease in patients with CTEPH, and it might predict gas exchange improvement after PTE. (*Circ J* 2008; **72:** 1136–1141)

Key Words: Bronchial artery; Chronic thromboembolic pulmonary hypertension; Pulmonary circulation; Pulmonary embolism

In patients with chronic thromboembolic pulmonary hypertension (CTEPH), dilatation of the bronchial arteries (BAs) is a well-recognized feature on conventional angiography[1] and computed tomography (CT) angiography[2,3] As the finding of dilated BAs is rarely seen in patients with idiopathic pulmonary arterial hypertension (PAH) or acute pulmonary embolism, it has been suggested that this feature could help distinguish patients with CTEPH from those with other diseases causing pulmonary hypertension[1,3,4]

The presence of dilated BAs represents increased systemic collateral blood supply[1,2] and it plays a important role in maintaining the viability of ischemic lung parenchyma after pulmonary artery occlusion[5] However, the mechanisms of bronchial arterial development are not well understood. It is thought that both hemodynamic and nonhemodynamic factors might be involved[6] In a canine model, Rehulova et al showed that the development of collateral bronchopulmonary circulation depended on the size of the occluded branch of the pulmonary arteries[7] In patients with CTEPH, the location of thrombi varies between individuals, but to our knowledge no study has evaluated the relationship between the location of thrombi and the dilatation of BAs in humans.

Previous studies showed a lower postoperative mortality rate and lower postoperative pulmonary vascular resistance (PVR) after pulmonary thromboendarterectomy (PTE) in patients with dilated BAs according to the preoperative evaluation, compared with patients without dilated BAs[8,9] Those studies classified patients into 2 groups, with (≥1.5 mm) or without (<1.5 mm) dilated BAs. Ley et al showed a correlation between the cross-sectional area of BAs assessed by CT angiography and the bronchopulmonary shunt volume assessed by magnetic resonance imaging[2] Those results prompted us to use the cross-sectional area of the BAs, instead of their diameters, for assessment of the relationship with surgical outcome after PTE, as the bronchopulmonary shunt volume may contribute directly to supporting ischemic parenchymal tissue caused by occlusion of the pulmonary arteries.

The purpose of our study was to use CT angiography to assess the relationship between the cross-sectional area of the BAs and the central extent of thrombi, as well as to evaluate the predictive value of dilated BAs for surgical outcome.

Methods

Study Population

For this retrospective study, we searched the computer database of Chiba University Hospital to identify patients

(Received January 16, 2008; revised manuscript received February 28, 2008; accepted March 11, 2008)

*Department of Respirology, Graduate School of Medicine, Chiba University, *National Hospital Organization, Chiba Medical Center, Chiba, Japan*

Mailing address: Hidefumi Shimizu, MD, Department of Respirology, Graduate School of Medicine, Chiba University, 1-8-1 Inohana, Chuou-ku, Chiba 260-8670, Japan. E-mail: shimizuhidefumi@gmail.com

with CTEPH (n=74) and PAH (n=19) who had undergone CT angiography between January 2002 and August 2007. All patients, except 1 with PAH, had undergone right-heart catheterization. The diagnosis of CTEPH or PAH was made on the basis of multiple diagnostic tests, including a detailed history, physical examination, pulmonary function testing, perfusion scanning, CT scanning, echocardiogram, right-heart catheterization and serologic tests.

Fourteen patients (11 with CTEPH, 3 with PAH) were excluded because of suboptimal contrast material delivery for evaluation of the BAs. Four patients with CTEPH were also excluded because the duration between CT angiography and right-heart catheterization was more than 3 months. Finally, 59 patients with CTEPH (CTEPH group) and 16 patients with PAH (PAH group: 8 with idiopathic PAH, 4 with PAH associated with collagen vascular disease, 2 with arterial septal defect and 2 with PAH associated with portal hypertension) were evaluated. Right-heart catheterization and selective pulmonary angiography were performed in all patients of the CTEPH group.

Twenty-four patients in the CTEPH group had undergone PTE; 2 of them died in the early postoperative period, and the remainder, except 1 patient (n=21), underwent post-operative CT angiography within 3 months (median [range], 1 [1–3]) after PTE. Postoperative blood gas analyses were performed for all patients and compared with preoperative blood gas levels.

As for the control of the total area of the BAs, we evaluated 12 patients who had acute pulmonary thromboembolism (APTE), whose thrombi were treated and resolved almost completely (post-APTE group).

The Human Subject Committee of Chiba University approved the study, and written informed consent was given by all patients at the time of diagnosis.

CT Protocol

All CT scans were obtained with a 16-row multidetector CT scanner (LightSpeed Ultra16; General Electric Medical Systems, Milwaukee, WI, USA) with 1.25-mm slice thickness. Patients were injected with 100 ml of contrast material with 350 mg of iodine/ml at 3 ml/s. All CT examinations were performed for a normal workup to diagnose or evaluate CTEPH or PAH, with a scanning delay of 20–30 s for optimal pulmonary artery visualization.

Image Interpretation

CT images were reviewed by 2 investigators using a cine-mode display on a computer workstation, and final evaluations were achieved by consensus. All BAs arising from the descending aorta in each patient as depicted by CT angiography were identified. At the mediastinal window setting of the axial images, right and/or left BAs were identified as contrast material-enhanced round or curvilinear structures (Fig 1). Their diameters were measured at the most proximal site from their origin. We calculated the cross-sectional area of each BA based on its diameter, and then summed the cross-sectional areas in each patient to yield the total area of the BAs.

The CTEPH group was divided into 3 subgroups, main type, lobar type and segmental type, according to the most proximal location of thrombi observed on CT angiography. The main type (n=9) was defined as thrombi of main arteries with or without more distal thrombi location, the lobar type (n=29) was defined as thrombi of lobar arteries with or without more distal thrombi location, and the segmental type (n=21) was defined as thrombi in segmental arteries or distal location.

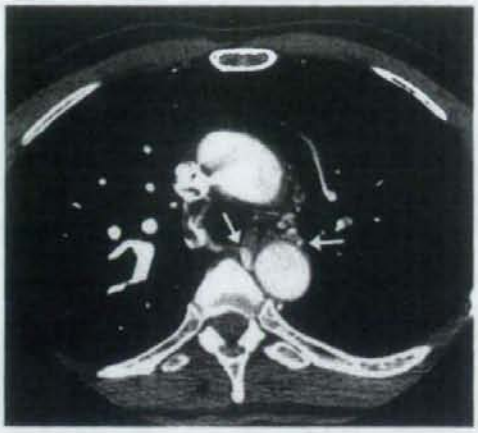

Fig 1. Computed tomography angiography in a patient with chronic thromboembolic pulmonary hypertension shows dilated bronchial arteries (arrows).

We also evaluated pulmonary infarction by the peripheral scar score as described by Heinrich et al[9]. In short, CT scan images at the lung window settings were analyzed for peripheral, irregular, wedge-shaped or linear densities. By adding up the number of involved lobes (lingual was regarded as a lobe), the peripheral scar score was obtained up to a maximum score of 6.

Statistical Analysis

Group comparisons were performed by Mann-Whitney U-test or 1-way analysis of variance on ranks (Kruskal-Wallis method) with post-hoc test using the Steel-Dwass method. When data were normally distributed with constant variance, correlations were measured using Pearson's correlation. Otherwise, the Spearman rank sum correlation was used. Comparison of the total areas of the BAs between before and after PTE was performed by Wilcoxon matched-pairs signed-ranks test. For all comparisons, a p-value of less than 0.05 was considered to indicate a statistically significant difference.

Results

Clinical and Hemodynamic Characteristics of the Patients

Table 1 summarizes the clinical and hemodynamic data from the 75 patients included in the current study. No statistical significant differences were found in terms of age, mean pulmonary artery pressure, cardiac index and PVR among the groups and subgroups.

Comparisons Between Patient Groups

The median total area of the BAs in the CTEPH group was significantly larger than that in the PAH group and the post-APTE group (Fig 2a: median [range], 6.9 [1.7–29.5] mm^2 vs 3.2 [0.8–9.4] mm^2 vs 2.0 [0.9–5.1] mm^2). When the CTEPH group was divided into 3 subgroups according to the most proximal location of thrombi, the median total area of the BAs in the segmental type was significantly smaller than in the other 2 types (Fig 2b). No significant difference in

Table 1 Clinical and Hemodynamic Characteristics of the 75 Patients in the Present Study

	PAH group (n=16)	CTEPH group			p value*
		All (n=59)	Main (n=31)	Lobar (n=18)	Segmental (n=13)	
Age (year)	50.4±16.6 (17–69)	54.9±12.2 (34–78)	60.2±9.4 (43–71)	53.7±12.6 (34–72)	54.4±12.4 (36–78)	NS
Sex (M/F)	2/14	16/43	6/3	8/21	2/19	
Mean pulmonary artery pressure (mmHg)	42.7±9.84 (26–55)	44.5±12.9 (23–71)	48.6±12.4 (32–70)	43.2±12.8 (23–71)	44.6±13.4 (23–71)	NS
Cardiac index ($L \cdot min^{-1} \cdot m^{-2}$)	2.73±0.53 (2.15–4.31)	2.56±0.63 (1.44–4.35)	2.36±0.91 (1.44–4.35)	2.46±0.54 (1.61–3.54)	2.79±0.58 (1.82–4.24)	NS
Pulmonary vascular resistance ($dynes \cdot s^{-1} \cdot cm^{-5}$)	694±202 (343–947)	828±425 (289–2,285)	986±467 (515–1,699)	839±468 (289–2,285)	746±368 (316–1,950)	NS

Data are mean±SD (range), unless otherwise stated.
**Study groups were analyzed by Kruskal-Wallis test.*
PAH, pulmonary atrial hypertension; CTEPH, chronic thromboembolic pulmonary hypertension; NS, not significant.

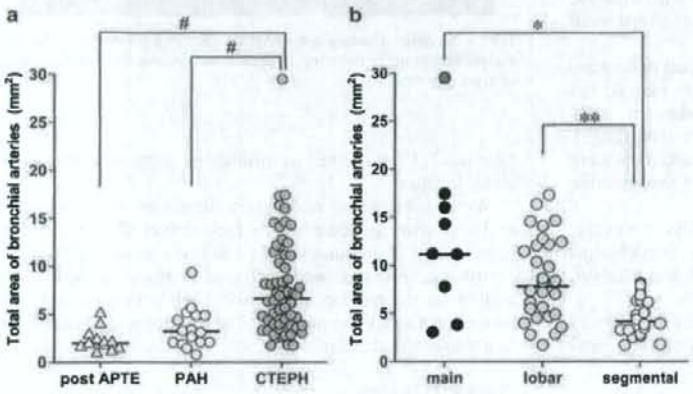

Fig 2. (a) Total area of the bronchial arteries in the post-APTE, PAH and CTEPH groups. (b) Comparison of the total area of the bronchial arteries in the 3 CTEPH subgroups according to the location of thrombi. Bars indicate median. #p<0.001, *p<0.01, **p<0.001. APTE, acute pulmonary thromboembolism; CTEPH, chronic thromboembolic pulmonary hypertension; PAH, pulmonary arterial hypertension.

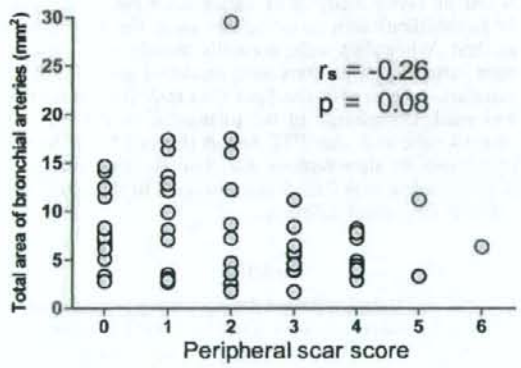

Fig 3. Correlation between peripheral scar score and total area of the bronchial arteries in the chronic thromboembolic pulmonary hypertension group.

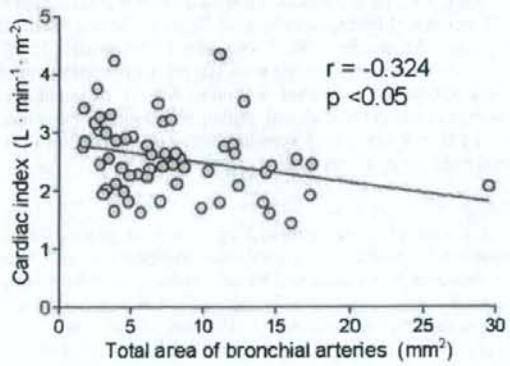

Fig 4. Correlation between the total area of the bronchial arteries and cardiac index in chronic thromboembolic pulmonary hypertension group.

total area of the BAs was observed between the PAH group and the segmental type of CTEPH. In the CTEPH group, the total area of the BAs showed a slight correlation with the peripheral scar score, but it did not reach statistical significance (Fig 3; r=–0.26, p=0.08).

Correlation With Total Area of BAs and Preoperative Hemodynamics

The total area of the BAs was significantly correlated with the preoperative cardiac index (Fig 4; r=–0.32, p<0.05). No significant correlation was found between the total area of the BAs and preoperative mean pulmonary artery pressure (r=–0.05, p=0.72) or PVR (r=0.12, p=0.37).

Table 2 Surgical Outcomes of Patients Undergoing PTE (n=22) and Correlation With Total Area of Bronchial Arteries

		Total area of bronchial arteries	
		r value	p value
Postoperative mean pulmonary artery pressure (mmHg)	26.5±12.5 (12–58)	−0.23	0.30
Postoperative cardiac index ($L \cdot min^{-1} \cdot m^{-2}$)	2.79±0.51 (1.85–3.63)	0.02	0.92
Postoperative pulmonary vascular resistance ($dynes \cdot s^{-1} \cdot cm^{-5}$)	388±348 (132–1,168)	−0.23	0.29
%reduction in pulmonary vascular resistance (%)	55±31 (−25–90)	0.16	0.47
Change in PaO_2 after PTE (mmHg)	14.1±13.6 (−10.9–44.3)	0.40	0.06
Change in $AaDO_2$ after PTE (mmHg)	−19.9±14.5 (−53.6–4.43)	−0.26	0.25

Data are mean±SD (range), unless otherwise stated.
PTE, pulmonary thromboendarterectomy; PaO_2, arterial oxygen tension; $AaDO_2$, alveolar-arterial oxygen pressure difference.

Correlation of Total Cross-Sectional Area of BAs With Outcome and its Change After PTE

Twenty-two patients (10 men, 12 women), mean 51.5 years (range, 18–69 years), underwent PTE and postoperative right-heart catheterization, and the relationship between the total cross-sectional area of the BAs and surgical outcome was evaluated. In this subgroup, the median total area of the BAs was 14.8 mm^2 (range, 3.6–29.5 mm^2). Every patient, except 1, had at least 1 BA with a diameter ≥1.5 mm. Based on the location of thrombi, 7 patients were classified as main type of CTEPH, 14 as lobar type, and only 1 patient was classified as the segmental type. Table 2 summarizes the surgical outcomes of the 22 patients. The total area of the BAs showed a slight correlation with changes in PaO_2, but it did not reach statistical significance (r=0.40, p=0.06). Other parameters regarding surgical outcome showed no correlation with the total area of the BAs. The total area of the BAs after PTE was significantly reduced compared with before PTE (Fig 5; median [range], 7.7[2.3–18.9] mm^2 vs 11.2[3.6–17.5] mm^2).

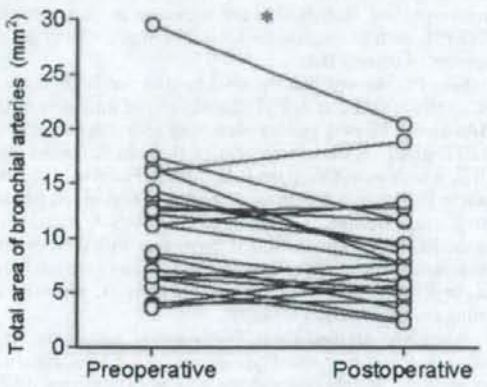

Fig 5. Comparison of the total area of the bronchial arteries before and after pulmonary thromboendarterectomy. *p<0.05.

Discussion

The current study demonstrated that the location of thrombi is related to the total cross-sectional area of the BAs in CTEPH patients. Although the BAs in the CTEPH patients were significantly dilated compared with those in the PAH patients, there was no significant difference in the total area of the BAs in the segmental type of CTEPH group and those in the PAH group. We also showed that the total area of the BAs in patients with CTEPH significantly decreased after PTE and might predict surgical outcome. With the advances in CT, the potential of CT angiography for diagnosing CTEPH has been demonstrated by a number of studies[10–13] Moreover, CT angiography is also being recognized as a useful test for evaluating the development of systemic collateral supply to the lung[2–4,8,9,14] Remy-Jardin et al showed that multidetector row helical CT angiography depicts the BAs more precisely than conventional angiography[14] Therefore, in the present study we also used multidetector row helical CT angiography to evaluate the dilatation of the BAs.

Consistent with previous studies[2–4,8,9,15] dilated BAs were frequently seen in the patients with CTEPH in the present study. The total area of the BAs in the CTEPH patients was significantly larger than that in the PAH patients. In the CTEPH group, as in earlier studies[8,9] we did not find any significant correlation between the total area of the BAs and the preoperative mean pulmonary artery pressure or the PVR, meaning that the severity of pulmonary hypertension was not a stimulus for the development of dilated BAs. However, the total area of the BAs was negatively correlated with the cardiac index. Although the onset of CTEPH is difficult to detect, disease duration might correlate with the development of dilated BAs. On the other hand, reduction in the cardiac index occurs in the symptomatic and decompensated phase of pulmonary hypertension[16] so disease duration might lead to this negative correlation between the total area of the BAs and cardiac index.

Of the CTEPH subgroups, the total area of the BAs in the segmental type was significantly smaller than in the other types. To our knowledge, this is the first study to investigate the correlation between BA enlargement and the central extent of thrombi in humans. The inverse relationship between the total area of the BAs and the peripheral scar score, possibly representing prior pulmonary infarction, might support this finding. One study using a dog model showed that the BAs did not become enlarged upon embolization of muscular arteries or arterioles, although enlargement occurred when the elastic branches of the pulmonary arteries were occluded? This suggests that occlusion of the pulmonary arteries at the proximal sites of bronchopulmonary arterial anastomoses might open them up. In humans, preexisting bronchopulmonary arterial anastomoses are commonly seen slightly proximal to the lobular arteries[17] The pressure gradient between the systemic arteries and the pulmonary arteries distal to the site of occlusion would increase when small distal arteries and arterioles are unaffected in patients with main or lobar type of CTEPH! and it would result in systemic arterial blood flow increasing in ischemic areas. Another possibility for the development of